The paper is a non-peer reviewed preprint submitted to Sedimentology

Article title: Microplastic deposition controlled by fluvial sedimentary facies in an urban river

Author names: Samuel Roudbar[1], Daniel P. Le Heron[1], Michael Wagreich[1], Ronald Pöppl[2]

Affiliations:

[1]Department of Geology, University of Vienna, Vienna 1090, Austria

[2]Institute of Hydrobiology and Aquatic Ecosystem Management, BOKU University, Vienna 1180, Austria

Corresponding author:

Samuel Roudbar samuel.roudbar@univie.ac.at

Room 2A350, Department of Geology, Josef-Holaubek-Platz 2, 1090 Vienna, Austria

Present address which is different from where the work was carried out

[2]Dr. Ronald Pöppl

Gregor-Mendel-Straße 33, 1180 Wien, Austria

Co-authors' email addresses:

Daniel Le Heron: daniel.le-heron@univie.ac.at

Michael Wagreich : michael.wagreich@univie.ac.at

Ronald Poeppl: ronald.poeppl@boku.ac.at

Abstract

Microplastic particles (MP) are characterised by their irregular shapes, lower density relative to natural grains, often failing at subscribing to sedimentological transport laws under controlled experimental conditions. Mismanagement of plastic waste, including associated environmental and health concerns, underpins the importance of systematic field-based behavioural observations on their riverine transport. Sediments from a highly anthropogenic river were sampled (N = 25) from 13 diverse sedimentary facies in the suburbs of Vienna to assess depositional patterns in terms of microplastic abundance and composition, sediment grain size distribution, total organic matter content (TOC), and seasonality. An alternative sedimentology-based grain shape classification, together with a new Depositional Capacity Index (DCI) were applied to determine preferential depositional patterns of MP. Microplastic abundance in river sediments reached 4,720 ± 4,644.5 MP kg^{-1} (mean ± SD, *n +17*) in spring and decreased significantly after the wet season to 1,606 ± 622.6 MP kg^{-1} (*n* = 8) in autumn. Deposition varies strongly across sedimentary facies and correlates with the newly DCI: throughflow-exposed riverbed with low DCI contained as little as 314 MP kg^{-1}, whereas vegetation-trapped backwater deposits with high DCI reached up to 15,544 MP kg^{-1}. Microplastics exhibit hydraulic size compensation relative to natural grains during transport, resulting in a systematic relationship between microplastic and sediment grain size. Their abundance is primarily controlled by sedimentary facies that favour the retention of organic matter, suggesting co-accumulation with organic-rich fine sediments, whereas microplastic composition (shape and density) shows no clear environmental control. These findings enhance our understanding of the environmental fate of microplastic particles as sediment analogues and help identify contamination hotspots relevant for targeted mitigation efforts.

Keywords

Microplastics, fluvial sedimentary facies, depositional energy, sediment transport, pollution

Highlights

- *An alternative sedimentology-based reclassification was applied to MP shapes*
- *A newly developed Depositional Capacity Index (DCI) ranks facies on the basis of their MP retention potential*
- *Systematic relationship between MP and sediment grain size is demonstrated*
- *MP deposition is governed by facies retaining high OM*
- *MP shapes (except rods) and densities are not controlled by environmental predictors*

1. Introduction

From remote mountain tops to deep-marine basins, microplastics have been detected across Earth's surface, with rivers acting as major continental transport pathways (Lebreton et al., 2017; Allen et al., 2019; Pohl et al., 2020). Microplastic particles (MP) are persistent environmental contaminants whose impacts have been shown to affect the biosphere across marine (e.g., Andrady, 2011), terrestrial (e.g., de Souza Machado et al., 2018), and riverine ecosystems (Hurley et al., 2017). Microplastics also pose potential risks to human health. More than 4000 chemicals associated with plastics have been classified as toxic, including substances that are carcinogenic, mutagenic, or toxic for reproduction (Monclús et al., 2025). A systematic understanding of the transport and deposition behaviour of this new and increasing anthropogenic particle class in fluvial environments is essential for improving waste management strategies and limiting environmental impact (e.g. Rohais et al., 2024; Arnon et al., 2025).

Sedimentologists can provide a crucial yet underutilized perspective in deciphering mechanisms controlling the transport, storage, and fate of plastic in the environment, as well as by improving particle description and transport dynamics (Waldschläger et al., 2022: Ghinassi et al., 2023; Rohais et al., 2024; Russell et al., 2025; Arnon, 2025; Liro et al., 2025). In geomorphology, sediment connectivity describes the efficiency of sediment transfer between sources and sinks within a system and influences facies development (e.g. Bracken et al., 2015). It provides a framework to assess human impacts on sediment availability in fluvial systems (Pöppl et al., 2017) and may aid interpretation of microplastic deposition patterns.

Microplastic transport displays similarities to sediment grain transport while also presenting significant differences, often observed under controlled experimental conditions. Microplastics are typically characterised by lower densities and higher shape diversity, resulting in a large variety of settling and rising velocities, significantly different from sediments (Waldschläger and Schüttrumpf, 2019). At the water-sediment interface, Schneidewind et al. (2025) showed that microplastic net deposition and near-bed transport cannot be well described by Stoke's law. However, under experimental aquatic bedload saltation conditions, Lofty et al. (2023) showed that spherical microplastics behave similarly to spherical sediment particles. Field-derived sedimentological data on microplastic transport and deposition will broaden the scope of laboratory and modelling results (Ibna Hafiz et al., 2025; Arnon, 2025).

Previous studies investigating the depositional behaviour of microplastics in fluvial sediments have typically focused on a limited number of depositional settings. High-density microplastics (MP) correlate positively with fine sand content in Warnow estuary sediments (Enders et al., 2019). Kiss et al. (2022) found point bars to be the most polluted in-channel facies along the Tisza River. Ghinassi et al. (2023) showed that bars, channel banks, and

vegetation-trapped deposits efficiently retain MP in the Arno River. Croiset et al. (2024) observed higher MP retention in semi-active channels of the Loire River, while Van Daele et al. (2024) demonstrated that mud and total organic content predict MP deposition in the Lys River. To date, a systematic comparison of MP occurrence, grain-size distribution and composition across sedimentary facies exhibiting different degrees of connectivity remains to be done.

In this study, 25 river sediment samples are evaluated for MP concentration, shape and size composition across 13 different facies varying in sediment grain size distribution and total organic content (TOC). The aim is to decipher relationships between MP behaviour and depositional energy regimes. A semi-quantitative Depositional Capacity Index (DCI) is presented allowing facies to be ranked for fine-grained sediment storage capacity proxying those that store microplastics. Samples were collected between April (n = 17) and October (n = 8) 2025 along the Krotenbach stream (Mödling, Austria), located downstream of a wastewater treatment plant (WWTP). The river was selected for its clear point source, elevated microplastic contamination, and limited lateral sediment inputs relative to upstream industrial and WWTP inputs, enabling field-based analysis of microplastic behaviour. A recent sedimentology-based microplastic grain shape scheme (Russell et al., 2025) was adopted and evaluated, and robust quality control procedures were implemented. This study aims to identify the key parameters controlling microplastic accumulation in river sediments by examining the roles of grain size, grain shape, polymer composition, and their co-occurrence with organic-rich depositional environments. Furthermore, the results improve our understanding of microplastic transport across the environment, and support risk mitigation and remediation strategies by characterizing facies with the highest contamination levels.

2. Regional Setting

2.1. Geological and geographical setting

Located in the suburbs south of Vienna, the Krotenbach is a small, highly anthropogenically impacted stream (Fig. 1). This classification is based on several key characteristics: (1) flow regulation by damming at a retention basin in Achau, where land is intentionally flooded for water management (Fig. 3F); (2) clear pollution evidence, including floating macro- and mesoplastic debris and large anthropogenic obstacles (Fig. 3E); (3) substantial wastewater input, contributing up to ~80% of total discharge (see SI.1.2); and (4) pronounced channel modification, including channelization and culverting, leading to river fragmentation (Best, 2019). The presence of the listed anthropogenic elements modifies sediment connectivity (Pöppl et al., 2017), particularly for fine sediments in which MP are preferentially found (e.g. Van Daele et al., 2024).

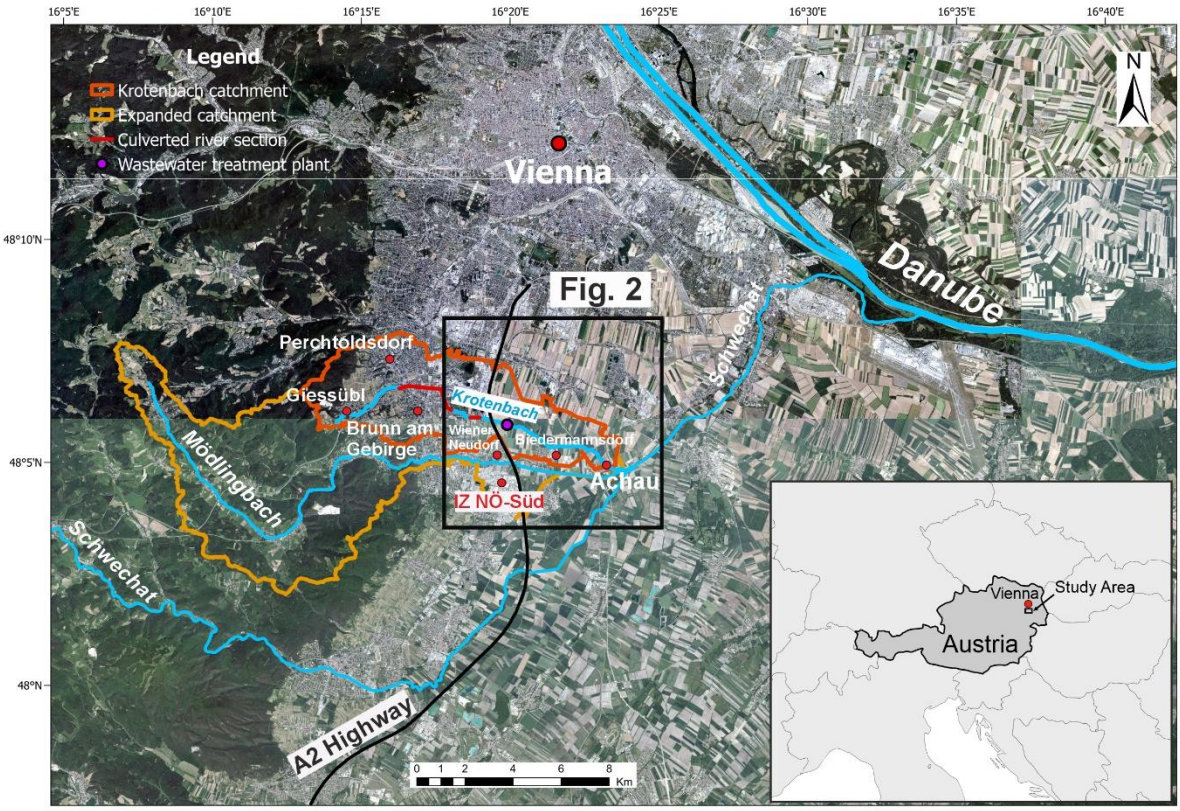

Fig. 1 Overview of the study area depicting the Krotenbach catchment and its expanded version once the contribution from the Mödlingbach is accounted for due to river splitting towards the mouth of the Krotenbach. Satellite images (Orthophoto 20 cm) retrieved from the Office of the Lower Austrian Provincial Government. Available at https://geoshop.noel.gv.at

The river is 14.29 km long, with a longitudinal channel gradient of 1.389% (368.8–170.4 m a.s.l.) derived from a DEM-based channel profile. Mean discharge at Achau (2023) was 0.272 $m^3 s^{-1}$, peaking at 0.995 $m^3 s^{-1}$ during floods (Austrian Hydrographic Service, eHYD, 2023). The 38.5 km^2 catchment is divided by the A2 motorway Austria (Fig. 1), with channel slopes of 2.158% upstream and 0.402% downstream.

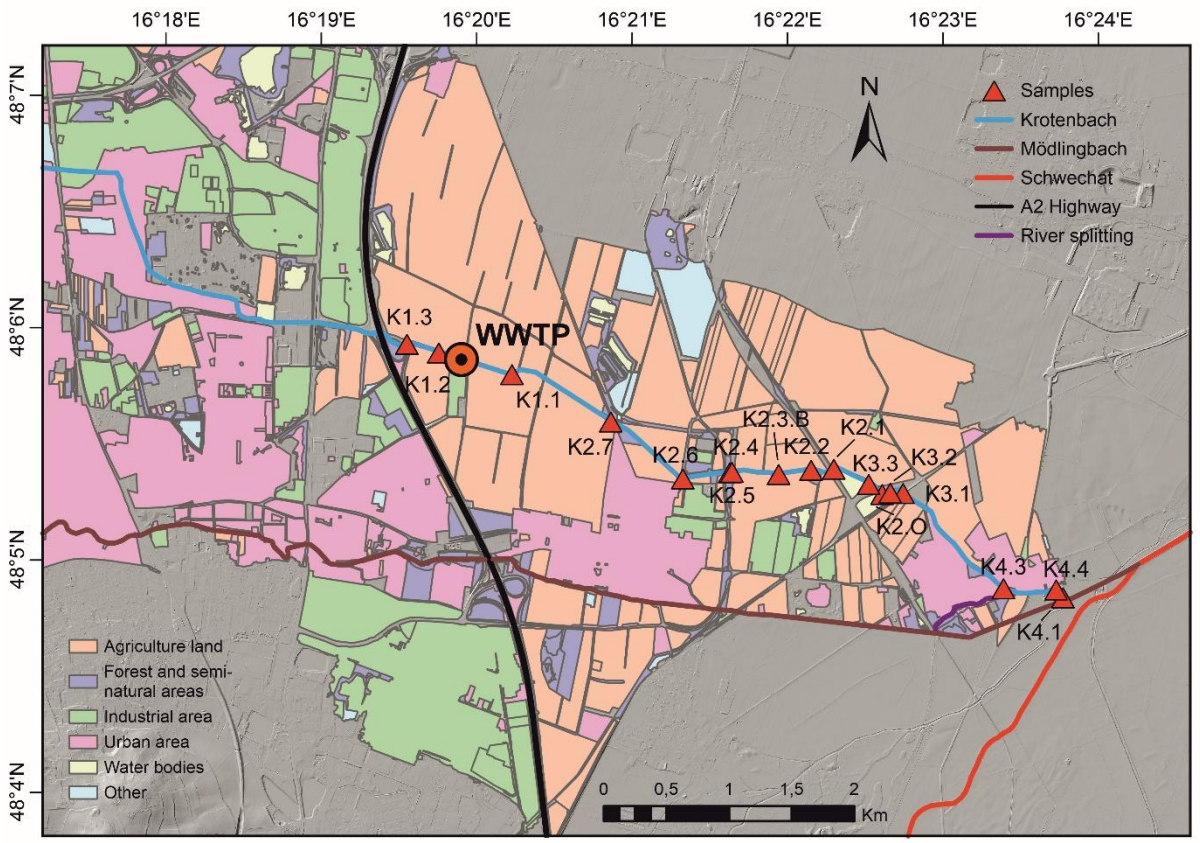

Fig. 2 Land use / DEM-combined map of the study area 14 km south of Vienna (Austria) in a straight line, showing the locations of the river sediment samples (red triangles) in the eastern half of the Krotenbach watershed. The orange-dotted circle denotes the position of the Mödling wastewater treatment plant (WWTP). The delimitation for the land use depicted is based on a watershed analysis for the Krotenbach river. DTM (1 m) retrieved from the Office of the Lower Austrian Provincial Government. Available at https://geoshop.noel.gv.at. Land use data retrieved from OpenStreetMap data provided by Geofabrik (Geofabrik GmbH, 2024)

A mid-reach riverbed sample (April campaign; central channel bed; dry sieving; sample 2.3A in SI.5) consists of poorly sorted, strongly coarse skewed very coarse sand to gravel (D_{50} = 2244.6 µm).

The stream is a single-thread, fully channelized system with a constrained, symmetric cross-section. This morphology reflects artificial confinement rather than intrinsic channel stability, as lateral mobility and adjustment are largely inhibited by engineering structures. The channel can therefore be described as a mixed-load system, with transport dominated by suspended fine-grained material (fine sand to clay) under conditions of relatively low sediment supply (after Schumm, 1985).

The Krotenbach is a low mountain range stream starting as a small creek called Hochleitenbach in the Wienerwald area close to the town of Giesshübl in Lower Austria (see Fig 1). Sediment source areas are in the northeastern-most foothill region of the Northern Calcareous Alps. Erosional facies in the steeper sections of the catchment are predominantly Upper-Cretaceous to Eocene clastic sediments (Gosau Group) and other mainly carbonate and minor siliclastic lithologies from the Permian to Lower Cretaceous of the Northern Calcareous Alps (Geologische Bundesanstalt Österreich, 2021). The watershed is also characterised by a major anthropogenic particle source area of microplastics in the IZ NÖ-Süd industrial zone (Fig. 1), the largest commercial area in Austria. MP enters the studied area through drifting, surface runoff, and loss from industrial activity just upstream of the sampling area (Waldschläger et al., 2020).

The stream flows under the urban area of Brunn am Gebirge and exits the underground channel on several occasions until reaching the agricultural areas between the towns of Wiener Neudorf, Biedermannsdorf and Achau, where it flows into the Mödlingsbach further southeast (Fig. 1). Sediment transport pathways are largely confined within (Upper) Holocene urban deposits before transitioning into Tertiary basins composed of synorogenic Upper Eocene to Miocene molasse sediments (Geologische Bundesanstalt Österreich, 2021). The reaches of the Krotenbach where the studied fluvial facies were sampled are situated within these basin fills.

Towards the watershed outlet, before entering Achau, the Mödlingbach splits in two, creating a side channel pouring about 10% (see SI.1.1) of the Mödlingbach discharge into the Krotenbach, before flowing all together into the Mödlingbach (Fig. 2). This means that for the last sample at the mouth of the river, the contributing watershed area is expanded (Fig. 1).

2.2. Flume-like field setting

Microplastics extracted from river sediments in this study are part of a well-defined source–pathway–receptor system (Waldschläger et al., 2020). The identified polymers likely originate from the IZ NÖ-Süd (Fig.1) and the WWTP (source), are transported along the Krotenbach (pathway), a highly anthropogenically impacted river, and are deposited in environmental compartments or temporary sinks (receptors) with varying depositional energy.

The main microplastic sources (excluding atmospheric deposition and agricultural inputs) are located within nine municipalities (~130,000 population equivalent), whose wastewater is treated at the Mödling WWTP at the upstream end of the study area (Stadtgemeinde Mödling, 2018). The WWTP discharges ~18,000 m³ of treated water daily into the Krotenbach, accounting for ~70–80% of total discharge (Stadtgemeinde Mödling, 2018; see SI.1.2). In addition to being a major point source of microplastics (e.g. Kay et al., 2018; Woodward et al., 2021), it sustains downstream flow, enhancing turbulence and remobilization of fine sediments.

The steeper reach west of the highway (Fig. 1) likely promotes mechanical fragmentation of plastics, whereas the downstream accumulation zone (Liro et al., 2025) favours deposition. This well-defined source and pathway, combined with continuous discharge into a

channelized stream, create conditions resembling a “flume-like field laboratory” for investigating microplastic deposition across sedimentary facies.

3. Methods

3.1. Sample collection

A total of 25 river sediment samples were collected (Fig. 2) for microplastic extraction, grain-size analysis, and total organic carbon (TOC) determination using pre-cleaned 330 mL glass jars (Ø: 60 mm). Seventeen samples were obtained on 9–10 April 2025, and the remaining eight samples were collected on 20 October 2025 to assess seasonal variability.

Meteorological data from the Brunn am Gebirge weather station, located upstream (Perchtoldsdorf, 291 m a.s.l., Fig. 1) of the Krotenbach section studied, indicate that 73.8% of the annual precipitation occurred during the six-month interval between sampling campaigns (GeoSphere Austria, 2025; see SI.2). This period therefore captures most of the annual rainfall and provides a representative framework for evaluating seasonal variability.

Facies were defined during a preliminary field campaign based on channel position, connectivity elements (e.g. large wood, obstacles; Pöppl et al., 2024), and the presence of fine-grained sediments. Samples were collected by scooping the upper 3 cm into glass jars or using a stainless-steel shovel. For submerged sites, jars were immersed perpendicular to flow and sealed underwater with a metallic lid to minimize contamination and loss of fines. Recovered sediment mass varied with site conditions (85.5–565 g; mean ± SD: 340.6 ± 143.1 g). All values refer to dry weight.

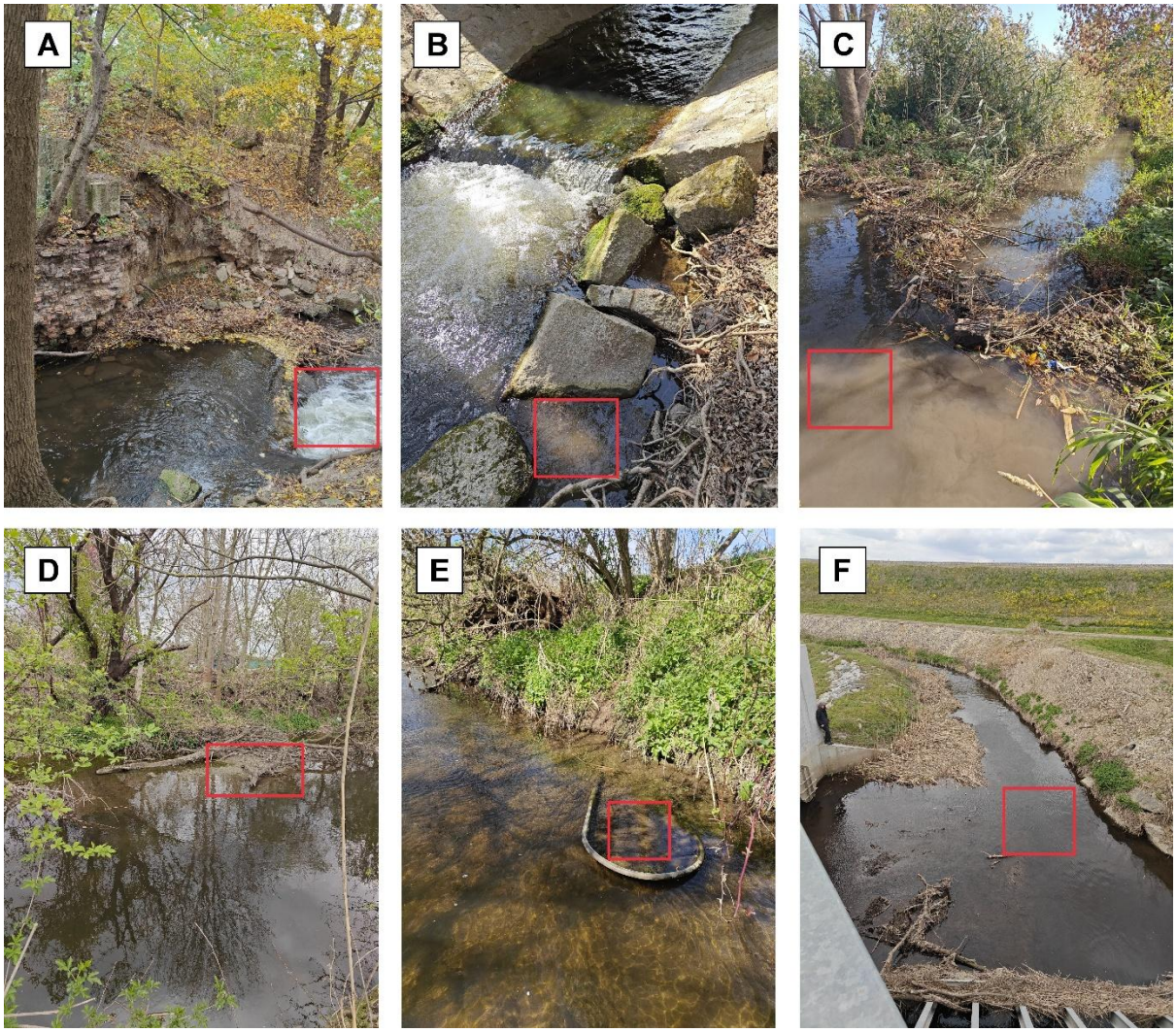

Fig. 3 Some of the depositional environments sampled along the Krotenbach with the red box highlighting the exact sampling location. (A) Plunge pool (KT2.4), (B) Pocket pool (KT2.6), (C) Backwater (KT1.2), (D) Vegetation-trapped in backwater setting (KT4.1), (E) Anthropogenic retention (KT2.3B), (F) Main channel bed with minor sheltering (KT3.1).

3.2. Facies-based depositional capacity assessment

To evaluate microplastic retention across depositional facies, environments were classified into 13 types based on geomorphological position, hydraulic setting, and sedimentological characteristics following standard fluvial facies concepts (e.g. Bridge, 2009; Miall, 2014). Each site was assigned a Depositional Capacity Index (DCI), defined as the sum of hydrodynamic exposure (HE) and hydraulic sheltering (HS) (Table 1), providing a semi-quantitative measure of flow exposure and shielding by channel obstacles. High DCI values

reflect low exposure, high sheltering, reduced sediment connectivity, and greater retention of fine sediment.

Table 1: Semi-quantitative basis for characterizing facies based on their hydraulic exposure and sheltering.

Score	Hydrodynamic exposure (HE)	Hydraulic sheltering (HS)
0	Thalweg/fully swept, strong turbulence, coarse lag, no fines	No shelter (open bed, no obstacles)
1	High exposure to stream flow, fines rarely persist	Minor shelter (small roughness, gentle margin)
2	Moderate exposure, fines patchy	Partial (bank proximity/vegetation causing some shielding)
3	Low-moderate exposure, fines commonly present	Strong shelter (bar lee side, embayment, local flow attenuation zone)
4	Low exposure, slack flow near margins/bar lee	Very strong shelter (behind large wood/boulders/structures; clear eddy zone)
5	Negligible exposure at baseflow (backwater/floodplain)	Effectively isolated (strong hydraulic separation)

HE and HS are complementary but distinct: HE represents broader flow exposure, whereas HS captures local attenuation (e.g. plunge pools may show high exposure but localized shelter, while channel margins may have low exposure but limited shelter due to channelization decreasing bed roughness). The index captures key hydraulic controls on sediment deposition and enables comparison among facies along the river profile. The robustness of the Depositional Connectivity Index (DCI) was further evaluated through a sensitivity analysis, the methodology and results of which are presented in Supplementary Information Section SI.6A and SI.6B.

3.3. Sample preparation

Samples were dried at 60˚C in a laboratory without forced-air convection until completely dry. Homogeneous mixing of the dry sampled was performed using a metallic spoon before sub-sampling according to dominant grain-size. Entire sediment aliquots (20 – 100 g dry

weight) were prepared for microplastic extraction to capture sample representativeness and proportion of fine-grained sediments. Between 50 and 200 g of dry sediments were prepared for grain size analysis. Duplicates of 100 mg of fraction finer than 125 µm were used for total organic content analysis.

3.4. Extraction of microplastics

The extraction workflow was designed to maximize polymer recovery from fluvial sediments while preserving particle integrity for subsequent FTIR identification. Individual processing steps follow widely applied principles in microplastic research but were adapted to the specific sedimentological characteristics of the study area. The method in this study is adapted from Zobkov et al. (2020) with the following modifications. No preliminary wet peroxide oxidization was undertaken to limit the early breaking down of larger organic particles, which could complicate subsequent FTIR analysis. The filter funnel cascade step is replaced by wet sieving into 63–500 µm and >500 µm, with 63 µm used as the lower identification threshold. Sieving was performed under tap water filtered to 40 µm. The wet fractions were vacuum filtered over 25 µm stainless-steel mesh prior to density separation.

Density separation was performed using a potassium formate solution (H_2O/KCOOH) with a minimum density of 1.45 g/cm^3. The 63-500 µm fraction underwent two to four density separation cycles (including manual stirring) over three days using 250 mL separation funnels. The >500 µm fraction was treated one to two times in tall, narrow 250 mL beakers (h: 12 cm; Ø: 6 cm). Potassium formate was selected as a safe, non-toxic, and cost-effective salt reagent that forms an alkaline solution that has been demonstrated to be suitable for microplastic extraction and subsequent FTIR analysis (Zobkov et al., 2020; Jarosz et al., 2022).

Following density separation, the supernatant was filtered over a 25 µm stainless-steel mesh. The retained fraction was transferred to a 1 L glass beaker containing 100 mL of deionized water and 50 mL of 30% H_2O_2 and left to react for 24 h. The solution was then sieved through a 63 µm sieve and rinsed back into the same beaker for Fenton digestion (applied to the <500 µm fraction only). The Fenton reagent consisted of 80 mL deionized water, 40 mL of 30% H_2O_2, and 20 mL of 0.05 M iron (II) sulphate heptahydrate ($FeSO_4 \cdot 7H_2O$; 15 g L^{-1}). The reaction proceeded for approximately 1 h on a magnetic stirrer at 400 rpm, with temperature continuously monitored to ensure it did not exceed 70 °C.

After organic matter digestion, the solution was rinsed with deionized water through a 63 µm sieve. Residual material was collected in a 100 mL glass beaker and vacuum-filtered onto Anodisc 25 (0.2 µm) filters (Whatman, Little Chalfont, UK). The >500 µm fraction was transferred into 50 mL of deionized water and examined using a stereomicroscope (1–10×; SMZ-U, Nikon, Shinagawa, Japan). Suspected microplastic particles were manually isolated and combined with the <500 µm fraction prior to final filtration. Two samples (KT2.6, KT4.1) were subsampled (50%) due to residual organic matter hindering spectral analysis.

3.5. Measurement and spectrographic data analysis

Anodisc filters (Ø: 25 mm) were analysed using a non-FPA micro-FTIR microscope operated in transmission mode (Lumos II, Bruker, Ettlingen, Germany). Particle identification was performed through manual mapping in OPUS 8.7.41, followed by individual spectral acquisition and comparison with two large polymer libraries i.e., KIMW (1191 entries) and siMPle (270 entries incl. most common organic material).

Prior to analysis, extensive training on organic-rich river sediments ensured reliable discrimination between synthetic polymers and natural material. Due to residual organic matter after extraction and long analytical times, 25% of each filter surface was

systematically mapped and analysed. Subsampling approaches are commonly applied in microplastic research and considered acceptable when representativeness is ensured (e.g. De Frond et al., 2023; see section 4.1. for recovery test results).

Microplastics were conservatively identified within 3200–1212.8 cm^{-1} and characterised by polymer type, morphology (elongation–flatness classification), and size (long-axis length; Fig. 4). In total, 59 polymer types were grouped into 16 categories (SI.3), each assigned an average density for analysis based on published data (Scientific Polymer Products Inc., n.d.; accessed December 2025). Spectral matches with HQ <400 were excluded, although such values may still indicate polymers. The mean HQ is 733.9. Raw spectra were analysed without pre-processing to minimize overestimation.

3.6. A novel microplastic grain shape classification

Upon identification MP were attributed a grain shape class based on their elongation and flatness observed in the FTIR live view optical image. This recent classification of Russell et al. (2025), which capture diverse plastic morphologies was slightly revised as six different grain forms were identified (previously four). The categories are rod (R), sphere (S), thin disc (DF), thick disc (DT), thin blade (BF), and thick blade (BT) (Fig. 4). This reclassification is tested and applied to study more precisely relationships between depositional environments and microplastic grain shapes.

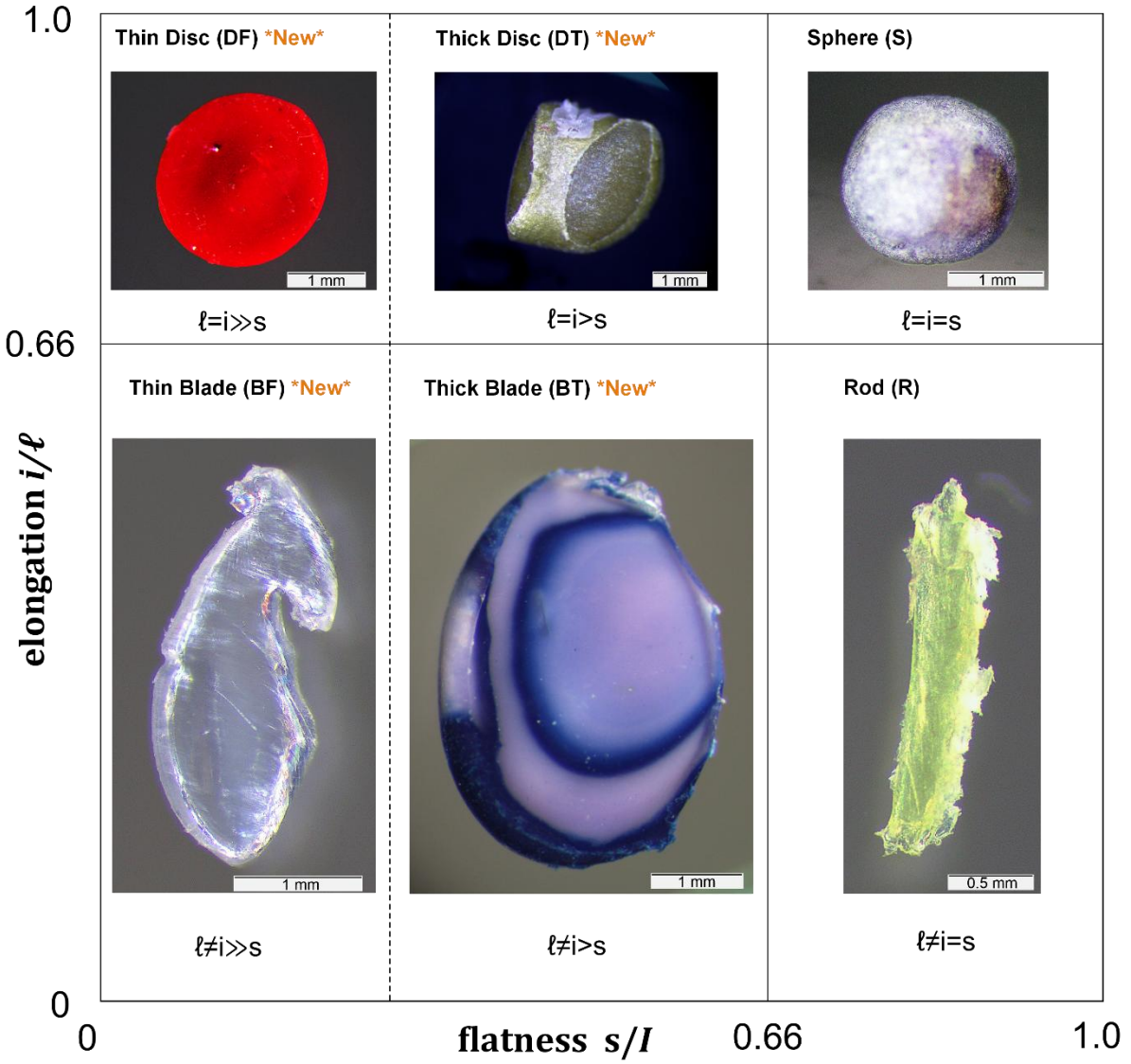

Fig. 4 Sedimentology-based microplastic grain shape reclassification that was applied in this study (adapted from Russell et al., 2025). The new shape classes specific to this study are highlighted.

3.7. Sediment grain size and total organic carbon analysis

Sediment grain-size distribution was determined by manual wet sieving using mesh sizes of 2,000, 1,000, 500, 250, 125, and 63 µm (corresponding to −1 to 4 φ). The <63 µm fraction (silt and clay) was collected in a container, dried, and weighed separately. Prior to sieving, samples were homogenized and treated with 15% H_2O_2 to promote grain separation and reduce organic matter content. Grain-size statistics were calculated following the method of Folk and Ward (1957). Total organic content (TOC), total inorganic content (TIC) and total carbon (TC = sum of TOC and TIC) determination was conducted on powdered sample

material using multiphase carbon and hydrogen/moisture determinator (RC612, LECO, St. Joseph, Michigan, USA). Microplastics themselves contribute organic carbon; however, given their negligible mass fraction relative to the total sediment mass, their contribution to measured TOC values was assumed to be insignificant.

3.8. Quality control and quality assurance (QA/QC)

Throughout this research, great care was taken to limit contamination levels and increase the quality of blank and spiked blank procedures to support the quality of microplastic data. Standard good practices during field and laboratory work were adopted such as the use of non-synthetic clothing, distilled water only, glassware, lab coat, and PFA (high density polymer above detection limit) wash bottles. All the liquid solutions prepared were vacuum filtered at 1.6 µm mesh size through glass microfibres filters. All the laboratory steps were performed by the first author in one room equipped with laminar flow cabinets except homogenisation and sub-sampling steps, which were taking place in a separate lab. FTIR measurements were performed in a different room with limited access to two people on average. Contamination and recovery levels were ensured by two field blanks (one per field campaign) and six spiked blanks. All the environmental samples were corrected for contamination levels found in the blank samples.

3.8.1. Field blanks

Field blanks were performed to account for microplastic contamination during sampling essentially coming from atmospheric deposition. They consist of a large (Ø: 75 mm) glass jars filled with 100 mL of distilled water that were left opened during sampling in the vicinity of the sediment facies. The two samples were relatively clean of organic matter and were directly filtered on Anodisc filters to avoid further lab contamination.

3.8.2. Laboratory contamination and extraction/analytical method quality evaluation

A novel procedure for assessing lab contamination and microplastic recovery rate was established to better simulate contamination and recovery potential of field-based samples. All blanks were made using sediments from the Krotenbach river of three different bulk grain sizes to reproduce the diversity in grain size of the facies-driven samples. Each blank was spiked with high-density polyethylene (PE) spheres (1.2 g cm^{-3}; 125–150 µm) at concentrations representative of those measured in the river sediments to evaluate the microplastic recovery rate of the adopted extraction method.

3.8.2.1. Laboratory blanks

Sediments recovered from grain-size analysis were grouped into three classes: (i) clay to fine sand, (ii) medium to coarse sand, and (iii) very coarse sand and coarser fractions. The material underwent density separation using a potassium formate solution (ρ = 1.45 g cm^{-3}) to remove most of the organic matter. The samples were subsequently dried and subjected to thermal decomposition at 450 °C for 5 h in a muffle furnace.

The three grain-size classes were then recombined in controlled proportions to produce artificial blank mixtures (duplicates per size class) with distinct dominant grain-size distributions. Each blank corresponded to the total dry mass of the field samples (30, 50, and 100 g). Mixing proportions followed a Gaussian distribution centred on the target dominant grain-size class (SI.4). For example, blanks dominated by the medium–coarse sand fraction consisted of 68.27% material within φ = 1–2, while the remaining 31.73% was equally distributed between adjacent coarser (φ = 0 to −1) and finer (φ = 3–5) fractions (15.86% each).

3.8.2.2. Recovery rates

Polyethylene (PE) microspheres (1.20 g cm^{-3}; 125–150 µm) were used as recovery standards (Cospheric LLC, Somis, California, United States). They were selected to represent small,

relatively dense particles, which are inherently more difficult to extract from environmental samples.

The PE microspheres were manually counted three times prior to spiking, and the mean count was used for each blank. Between 182 and 258 particles were added per blank before initiating the extraction procedure; the concentrations are comparable to those found in the field samples.

3.9. Statistical analysis

Statistical analyses were restricted to the April campaign, as lower microplastic counts in October limited statistical robustness; October data were excluded from correlation, ordination, and regression analyses. Figures were produced in R (ggplot2, dplyr, vegan) after data preparation in Microsoft Excel. Linear relationships were assessed using slope (β_1), R^2, and p-values. As data were often non-normal, included ordinal indices, and were expected to be monotonic, Spearman correlations (ρ) were also calculated.

Cluster analysis (Fig. 11) used Bray–Curtis distances based on microplastic shape proportions to examine compositional variation along the DCI gradient, treated as continuous. Group differences were tested using PERMANOVA (adonis2, 9,999 permutations; Anderson, 2001), dispersion with betadisper, and Mantel tests assessed correlations between compositional dissimilarity and DCI distance.

Detrended correspondence analysis (DCA) yielded a first-axis gradient length of 0.91 SD, indicating short gradients and supporting linear constrained ordination. As shape composition is proportional multivariate data, Bray–Curtis dissimilarity was used and distance-based redundancy analysis (dbRDA) applied instead of classical RDA (Legendre and Anderson, 1999).

Microplastic abundance was excluded from dbRDA, as it is not compositional. Instead, multiple linear regression tested effects of TOC, MzSED, DCI, and %finer63 on concentration. Variance inflation factors were low (VIF < 4), indicating no problematic multicollinearity and allowing all predictors to be retained (Zuur et al., 2009).

4. Results

4.1. QA/QC results

Field contamination levels are very low: between 2.9 and 14.6 MP kg^{-1}. Mean laboratory contamination across the six procedural blanks amounted to 2.77 PS particles kg^{-1}, 8.33 ELAS-L particles kg^{-1} (low-density elastomers), and 41.66 PES fibres kg^{-1} (PES fibres). Overall recovery of PE microspheres (1.20 g cm^{-3}; 125–150 μm) averaged 87.6 ± 6.83%. The highest recovery was observed in blanks dominated by very coarse sand to coarse gravel (96.02%), whereas the lowest recovery occurred in blanks dominated by very fine to fine sand (78.57%). The analytical strategy of mapping only 25% of the filter surface was also evaluated. Analysis of 25% of the filter yielded a reproducible recovery of 25.9 ± 2.22% of the recovered PE microspheres, consistent with the proportion of filter area examined (all results from QA/QC are available in SI.4).

4.2. Facies description and semi-quantitative ordering

This study identified thirteen facies based on their position with respect to the channel, hydraulic energy regime and interpreted depositional process (Table 2). The results from the sediment grain distribution corroborate the initial depositional description across the studied river section except for the backwater (KT1.2; Fig 4C) with Mz = -0.37, a very-coarse graphic mean for a depositional setting favouring the settling of fine-grained sediments. The pocket pool facies, located near a small step (Fig. 3B) with increased bed shear stress, is

unexpectedly strongly coarse-skewed. Apart from the vegetation-trapped deposit at the river mouth (Fig. 3D) and the plunge pool facies (Fig. 3A), which are moderately sorted silt and very coarse sand, respectively, all facies are poorly to very poorly sorted, ranging from silt to granules and pebbles. Detailed grain-size data for each site are provided in the SI.5.

Table 2: Facies description and sediment grain analysis

Facies	**Channel position**	**Mz (ϕ)**	**Sorting (σ1)**	**Skewness**	**Hydraulic energy regime**	**Depositional process**
Pocket-pool retention (anthropogenic)	Adjacent to bank between cut stones	0.43	2.48	Strongly coarse skewed	Very low; lateral recirculation	Localised suspension settling
Floodplain overbank	Beyond bankfull channel	2.60	2.48	Strongly fine skewed	Very low; inundation-dependent	Suspension settling during overbank flooding
Backwater	Low-velocity zones behind obstruction	-0.37	1.90	Strongly coarse skewed	Low; suspension-dominated	Suspension settling under reduced flow velocity
Vegetation-trapped (channel-margin)	In the lee of organic obstacle adjacent to bank	-0.71 – -0.63	1.18 – 1.37	Strongly coarse skewed	Low; roughness-enhanced deceleration	Flow attenuation by vegetation, fine sediment interception
Vegetation-trapped (backwater)	In the lee of organic obstacle before the river mouth	4.13	0.76	Strongly fine skewed	Low; roughness-enhanced deceleration	Flow attenuation by vegetation and backwater, fine sediment interception
Pool-margin	Edge of scour pool	2.00	2.51	Strongly fine skewed	Low along margins; higher in pool center	Settling from suspension along shear gradient

Anthropogenic retention (Fig 2.; E)	Inside bathtub-like adjacent to bank	0.22	1.76	Coarse skewed	Low to moderate; Locally reduced with sieving effect	Artificial deceleration; induced sediment trapping
Backwater-influenced main channel bed	Channel bed within a reduced-velocity reach	3.69	1.44	Strongly fine skewed	Low to moderate; less than normal main channel conditions	Reduced bedload transport; enhance fine retention
Lateral accretion bar	Inner bend of meander	1.72 – 3.64	0.95 – 1.27	Fine to coarse skewed	Moderate; decreasing flow velocity across bar surface	Helical flow-driven lateral accretion; bar mitigation
Channel-margin bar	Adjacent to banks	-1.11 – 0.87	1.23 – 1.88	Coarse to strongly coarse skewed	Moderate; velocity gradient from channel core	Lateral deceleration and bar accretion during falling stage
Mid-channel bar	Central channel, emergent or submerged bar	0.62	1.43	Symmetrical	Moderate to high; flow bifurcation	Bar growth during reduced discharge; reworked during floods
Main channel bed	Thalweg or active channel floor	-1.43 – 0.43	0.63 – 1.6	Symmetrical to strongly coarse skewed	High; transport-dominated; frequent competence exceedance	Bedload transport and episodic deposition during waning flow
Plunge-pool	Immediately downstrea	-0.96	0.82	Strongly coarse skewed	Very high locally; turbulent	Scour and hydraulic

	m of step, obstruction, or drop					sorting; lag concentration

The hydraulic exposure (HE) and hydraulic sheltering (HS) values are summarized in Table 3 and summed up to assign a normalized (0-1) DCI value per sampling site. The semi-quantitative ranking highlights the diversity of facies of the sampling campaign.

Table 3: Hydrodynamic exposure (HS) and hydraulic sheltering (HE) attributed (0-5) per described facies

Sample ID	**Facies**	**HE**	**HS**	**DCI (normalised)**
KT2.6	Pocket-pool retention (anthropogenic)	5	5	1
KT2.0	Floodplain overbank	5	5	1
KT1.2	Backwater	4	4	0.8
KT3.2	Lateral accretion bar	4	4	0.8
KT4.1	Vegetation-trapped (backwater)	4	4	0.8
KT2.2	Vegetation-trapped (channel-margin)	4	3	0.7
KT2.3B	Anthropogenic retention	3	3	0.6
KT2.5	Pool-margin	4	2	0.6
KT1.1	Lateral accretion bar	2	3	0.5
KT2.1	Channel-margin bar	3	2	0.5
KT3.3	Vegetation-trapped (channel-margin)	3	2	0.5
KT4.3	Channel-margin bar	3	2	0.5
KT1.3	Backwater-influenced main channel bed	3	1	0.4
KT2.7	Mid-channel bar	1	2	0.3
KT2.4	Plunge-pool	1	1	0.2
KT3.1	Main channel bed	1	0	0.1
KT4.4	Main channel bed	1	0	0.1

4.3. Microplastics abundance and composition

In April 2025, MP abundance is spreading almost two orders or magnitude along the river section (Fig. 5) ranging from as low as 314.3 MP kg^{-1} (KT4.4) to 15,544.3 MP kg^{-1} (KT4.1) despite being only a few hundred meters apart (Fig. 2). The mean microplastic concentration for April is 4,719.9 ± 4,644.5 MP kg^{-1} (SD, n = 17). Riverbed and plunge pool facies, characterised by high sediment connectivity, exhibit the lowest microplastic abundances

(314.3 – 1,064.3 MP kg^{-1}), whereas overbank, pocket pool, and vegetation-trapped facies associated with low connectivity show the highest values. (8,794.3 – 15,544.3 MP kg^{-1}). There is an increase in microplastic abundance after the WWTP located between sampling sites KT1.2 (2,752.65 MP kg^{-1}) and KT1.1 (5,677.65 MP kg^{-1}) despite having a relative decrease in depositional capacity from 0.8 to 0.5 according to the computed index (Table 3).

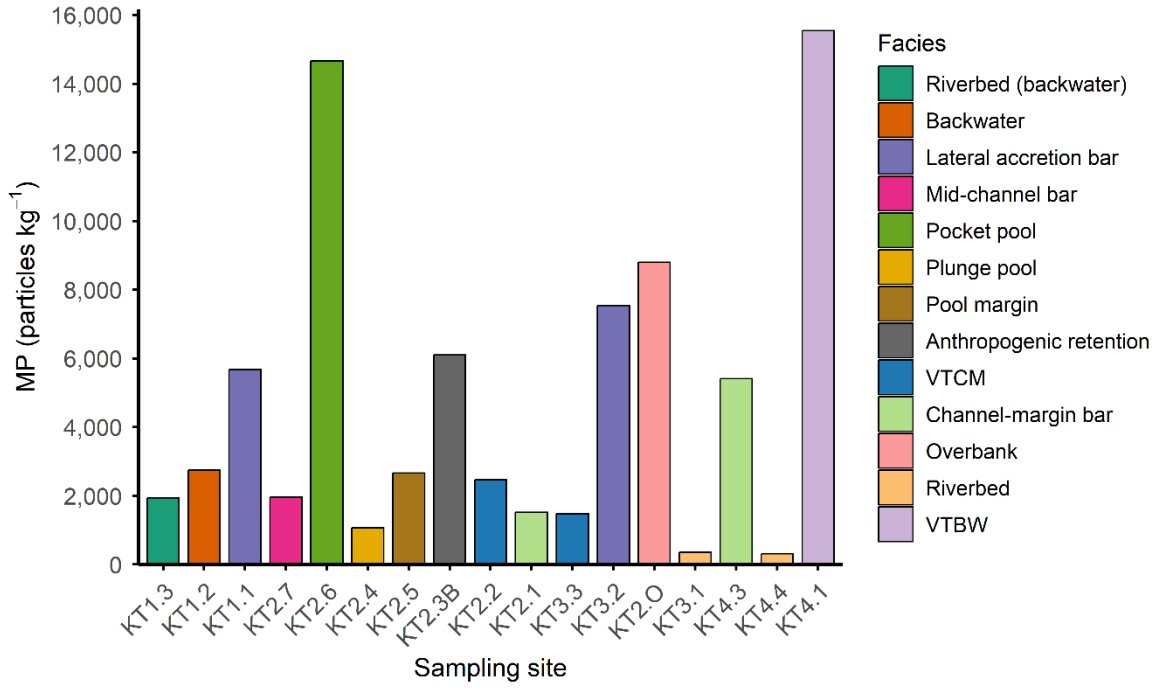

Fig. 5 Microplastic abundance (MP kg^{-1} of dry weight sediments corrected for all blanks) per sampling site colored by facies and ordered downstream from the April 2025 campaign. The wastewater treatment plant is located right after sample KT1.2. VTCM: Vegetation-trapped deposits at the channel margin. VTBW: Vegetation-trapped deposits in backwater setting.

Polystyrene (PS) (35.4%), polyethylene (PE) (16.4%), and polypropylene (PP) (15.4%) are the most common polymer types, all three characterised by theoretically buoyant properties (Fig. 6). Non-buoyant or relatively higher density microplastics with a density higher than 1.15 g cm^{-3} represent 19.42% of the total polymer particles identified. In total, 517 microplastic particles were identified from the first field campaign. Thin blades (23.79% of total), rods (19.15%), and thick blades (18.37%) are the most common. Their respective median long-axis size is 206 µm [145 – 292 µm], 506 µm [346.5 – 749.5 µm], and 177 µm [137.5 – 270.5 µm]. The measurements for the three other shapes are 101 µm [83 – 146.25

µm] (n = 88) for thick disks, 110 µm [89 – 146 µm] (n = 69) for thin discs, and 96 µm [79 – 120.5 µm] (n = 43) for spheres. Polystyrene is by far the most represented polymer with dominant grain-shape approximating thick discs. Thick discs define 17.02% of all grain-shapes, while PMMA are almost exclusively represented by spheres, sphere being the least common grain-shape characterizing 8.32% of all microplastics. Rods are the dominant and almost exclusive shape describing higher-density PET and PES polymers.

Eight sites from the April 2025 field campaign were analysed to evaluate the seasonality effect of microplastic deposition and composition in October 2025. Mean microplastic concentration for October is 1,606.2 ± 622.6 MP kg^{-1} (SD, n = 8). Abundance levels are significantly lower by 44.16% on average between the two sampling campaigns after excluding sampling site KT4.4S; the only sample exhibiting a major increase in microplastics occurrence (Fig. 7). The observed relative increase reflects a shift in the depositional facies sampled, driven by changes in water level. Sample KT4.3S (channel bed margin) shows a 77.45% decrease in microplastic abundance.

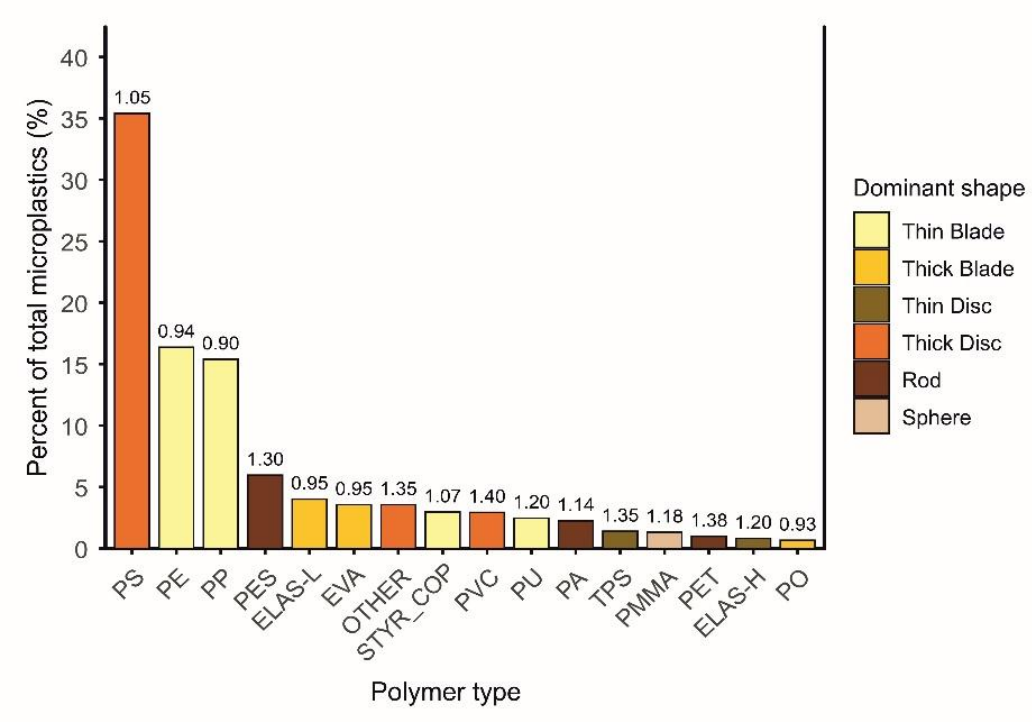

Fig. 6 Proportions of each polymer type colored by their dominant shape found across all samples. The top annotation is the polymer' specific density (g cm^{-3}). ELAS-L and ELAS-H are reclassified polymer categories standing for low-density and high-density elastomers respectively. STYR_COP is another reclassified category consisting of styrene-based polymer with distinct IR spectra from polystyrene (PS). OTHER includes high-density polymer that were rarely identified during the analysis. The PO group contains different polyolefin types of plastic. All the details of the reclassification can be found in SI.3.

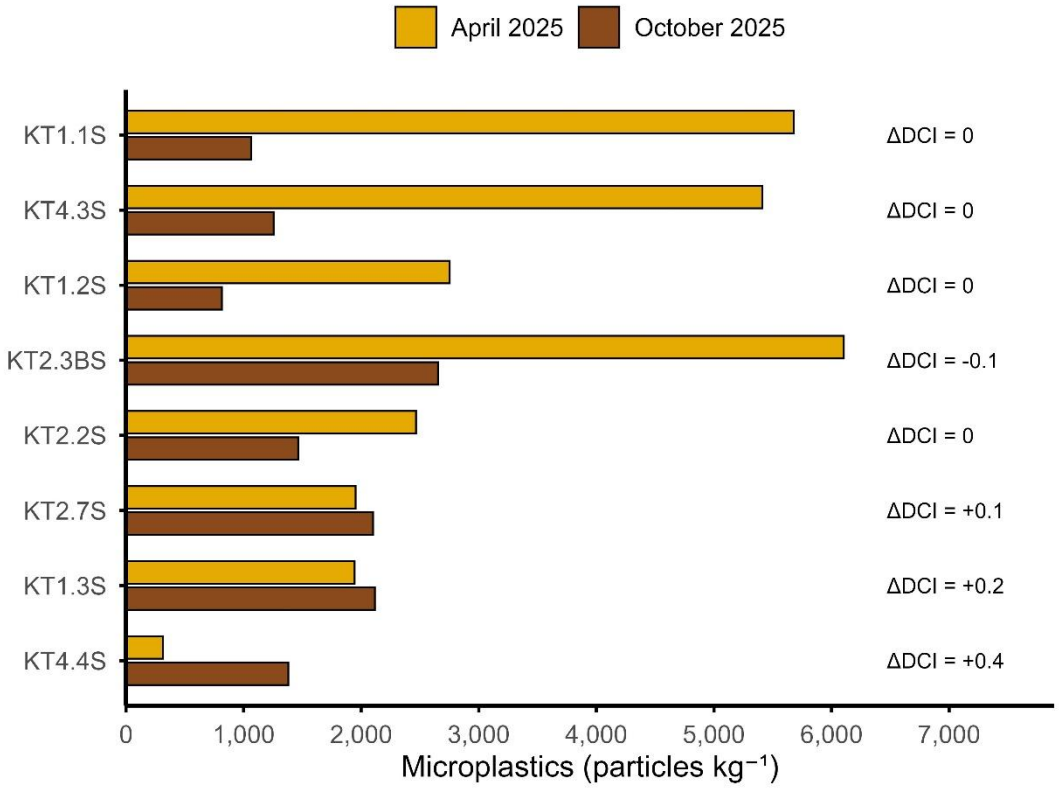

Fig. 7 Seasonality effect on microplastics abundance among eight resampled facies between April 2025 and October 2025. A net decrease in microplastic particles kg^{-1} is depicted after the rainy season. Annotations of the change in depositional capacity index (DCI) between the two sampling campaigns are shown.

Given the marked decrease in microplastics abundance found in river sediments in October 2025, the reduced number of sites sampled, and the lack of significant preliminary correlations between response and predictor variables, descriptive and inferential statistics were restricted to the first sampling campaign.

Graphic means of MP long axes and sediments across all samples display a perfect linear regression (R^2 = 0.988; p = 6.47 e-16) (Fig. 8; SI.5). The relationship between their size is described by $Mz_{MP} = 83.274 + 0.328\, Mz_{Sed}$ indicating that microplastics are systematically sorted in bulk sediments that are 3.3 times larger

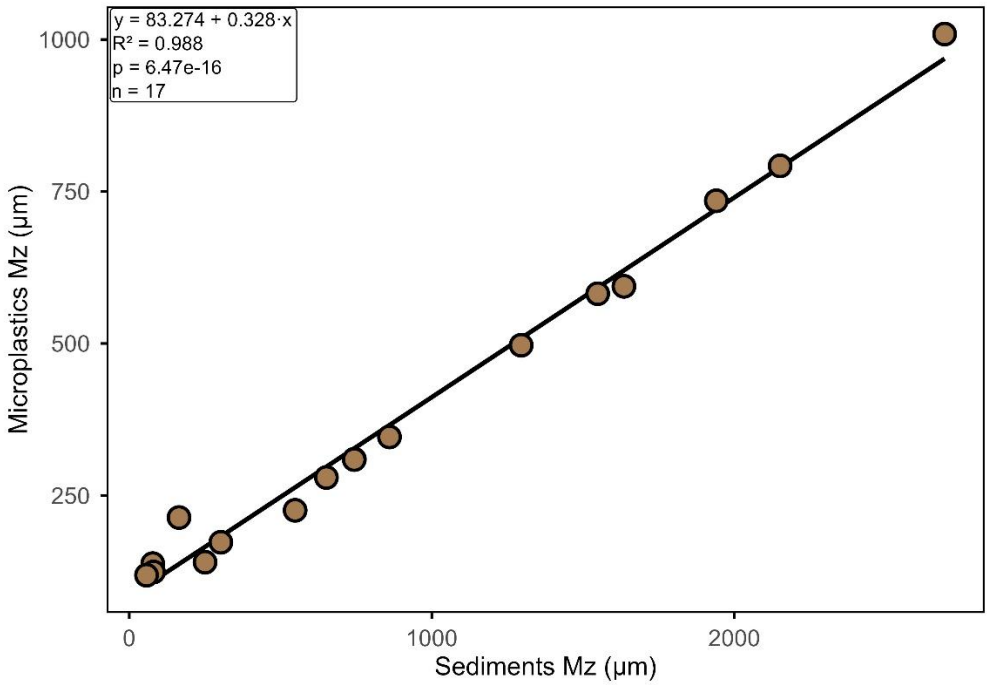

Fig. 1 Sediment graphic mean against microplastic graphic mean in µm.

4.4. Relationships between microplastic abundance and predicting variables

Microplastics abundance across all facies is plotted against two predictors, i.e. the percentage finer than 63 µm (silt/clay) (Fig. 9A) and the total organic content (Fig. 9B) of the bulk sediments. Both variables show a positive relationship with microplastic abundance, although their predictive strength differs. Preliminary correlation analyses suggest that the total organic content of bulk sediments is a better predictor of microplastic occurrence across all facies than the silt/clay content. When outliers are excluded from the regression model, the relationship between microplastic abundance and silt–clay content strengthens markedly, with the coefficient of determination increasing from $R^2 = 0.33$ to $R^2 = 0.69$ (Fig. 9A). In contrast, the relationship with TOC shows only a modest improvement ($R^2 = 0.59$ to $R^2 = 0.66$). Most correlation displayed (Fig. 9B) are statically significant (p-value < 0.05); however, the Spearman correlation between TOC and MP abundance becomes non-significant after excluding outliers. This change is accompanied by a reduction in the regression slope (from 1786.2 × TOC to 1607.5 × TOC), indicating a weaker monotonic association between TOC

and microplastic abundance. Relationships between microplastic concentration and sediment sorting, skewness, and kurtosis were weak to absent. Sorting showed a moderate positive Spearman correlation (Spearman $\rho = 0.46$, $p = 0.061$), whereas skewness and kurtosis exhibited no meaningful relationships (Spearman $\rho < 0.12$, $p > 0.39$)

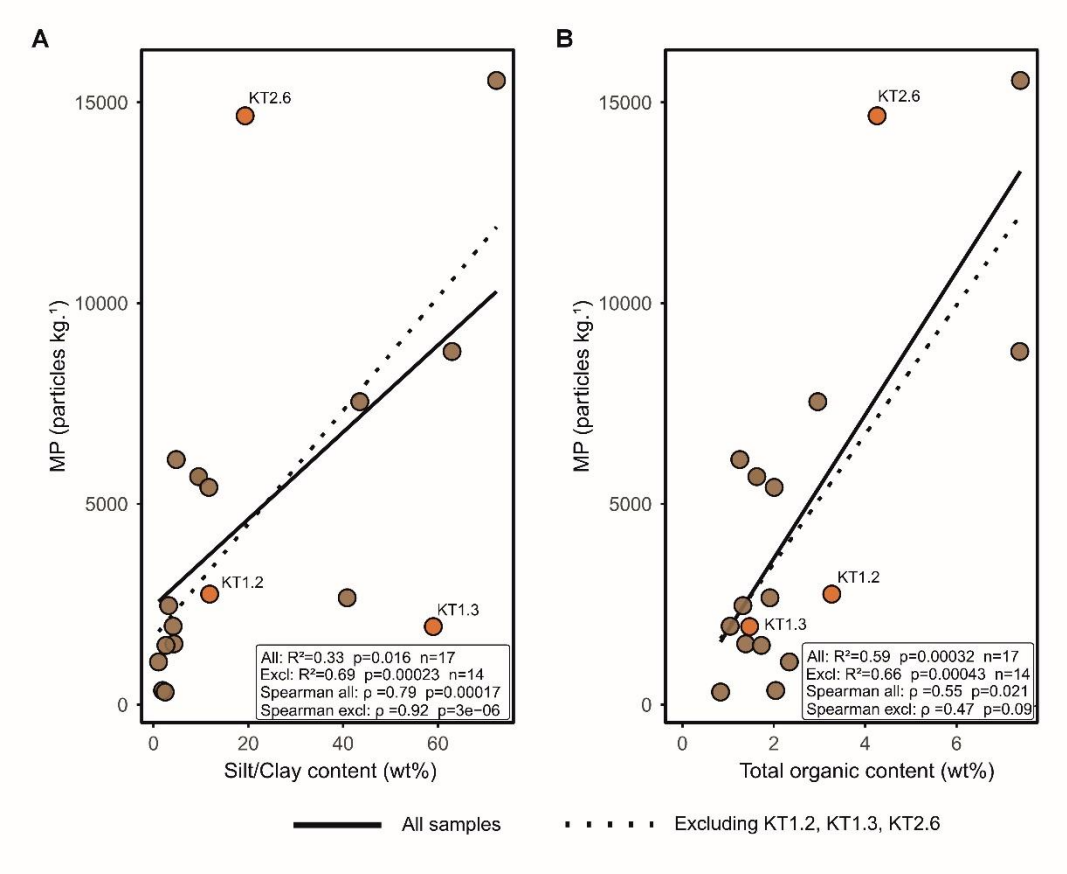

Fig. 9 Microplastic particles kg^{-1}are plotted against silt/clay content (A) and total organic content (B). Outliers (KT1.2/KT1.3/KT2.6) are colored orange. Two regression lines per plot are fitted to visualize the effect of excluding outliers on the correlation between with the two predicting variables.

The semi-quantitative depositional capacity index (DCI) developed in this study explains robustly ($R^2 = 0.78$; $p = 1.3e\text{-}05$) a monotonic increase in microplastic abundance with an increase in DCI values across facies located downstream the WWTP (Fig. 10). The graphic mean of the bulk sediments does not systematically decrease with increasing microplastic occurrence. However, the highly contaminated sites are generally characterised by relatively smaller sediment graphic mean (Fig. 10). Strongly fine skewed high DCI facies such as the vegetation-trapped silt deposits at the mouth of the river (Fig. 3D) and overbank fine sand

deposits retain the some of the highest microplastic values, 15,554.3 MP kg^{-1} and 8,794.3 MP kg^{-1} respectively. Lateral accretion bars at KT1.1 (DCI = 0.5) and KT3.2 (DCI = 0.8) differ in DCI values because the former experiences a strong flushing effect from WWTP outlet whereas the latter is markedly sheltered behind a man-made meander in the Krotenbach retention basin. This difference in depositional capacity is reflected in their microplastic retention, i.e. 5,677.7 MP kg^{-1} and 7,544.3 MP kg^{-1} respectively. Strongly coarse skewed coarse sand deposits from the pocket pool facies also exhibit a very high storage of microplastics (14,464.3 MP kg^{-1}) and the highest DCI value. The "metal bath" (KT2.3B) lying at the margin of the channel (Fig. 3E) is a depositional environment favouring microplastic deposition as well (6,104.3 MP kg^{-1}). Facies characterised by low DCI values such as main channel riverbed and plunge pool facies also exhibit low microplastic counts (between 314.3 and 1,064.3 MP kg^{-1}).

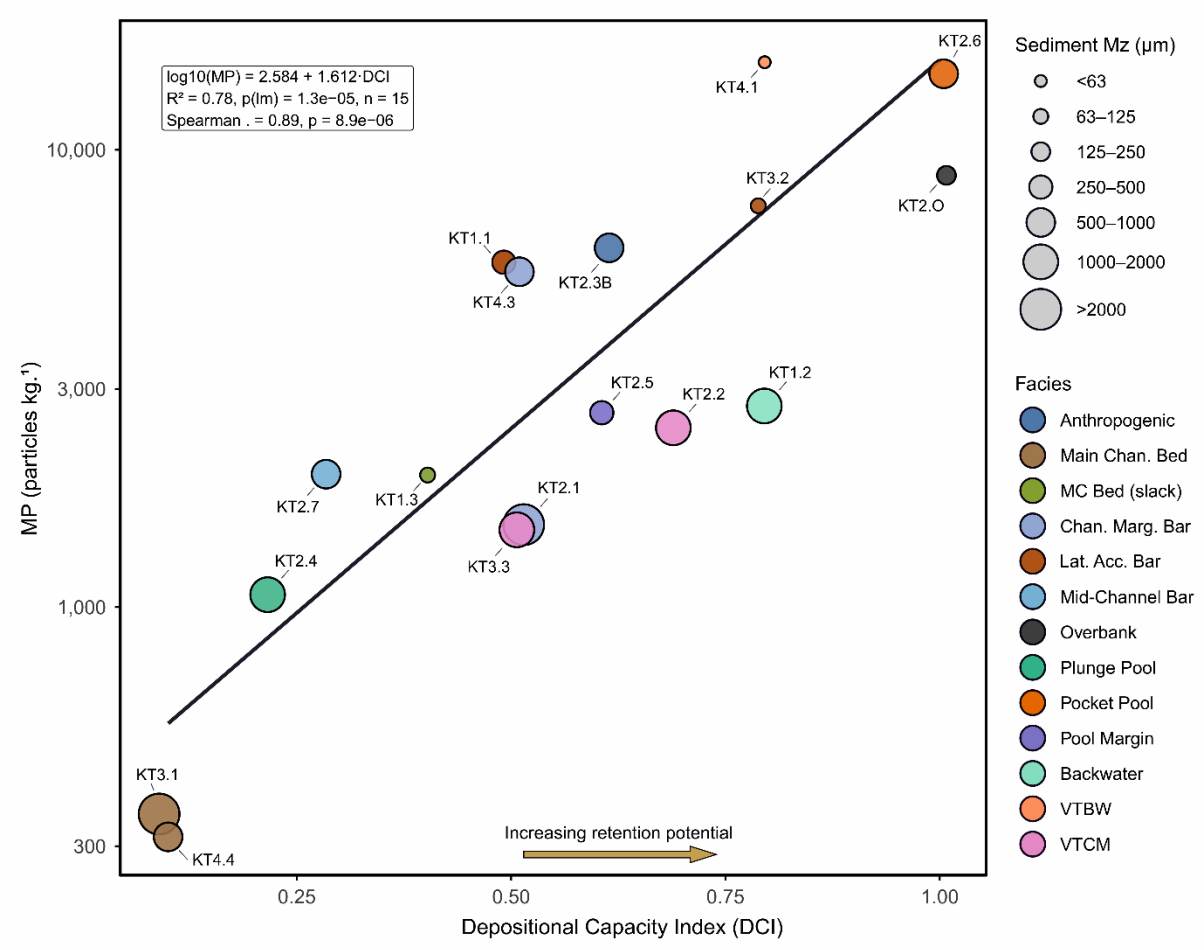

Fig. 10 Relationship between depositional capacity index (DCI) and microplastic abundance (log transformed) excluding sites upstream of the wastewater treatment plant. Points are colored by facies and represented in size according to their graphic mean. VTBW stands for vegetation-trapped deposits in backwater setting and VTCM for vegetation-trapped deposits in channel margin setting. MC stands for main channel.

Statistically, as a model testing multiple linear regressions, the predictors described above (TOC, $\%finer_{63}$, Mz_{Sed}, DCI) explain 75% ($R^2_{adjusted} = 0.67$, $p = 0.001$) of the variance in microplastic abundance across all sites and is deemed statistically significant ($\sigma = \pm$ 2,600 MP kg^{-1}, F = 9.22). Investigating predictors individually reveals that only TOC has a statistically significant positive (β = 1,566.6, $p = 0.022$) effect on MP abundance and is the strongest predictor in the model (Table 4). Mz_{Sed} is not significant ($p = 0.096$) but suggests that coarser sediments may reduce MP abundance (β = -2.27). DCI has a strong positive effect (β = 4986.6) but is not statistically significant (p = 0.168) when other variables are included. The least significant predictor is $\%finer_{63}$ ($p = 0.247$) (Table 4).

Table 4: Multiple linear regression on microplastic abundance. TOC stands for total organic content, Mz_{SED} is the graphic mean of the bulk sediments, DCI is the Depositional Capacity Index and $\%finer_{63}$ corresponds to the mass percentage of sediments smaller than 63 µm.

Variable	***β* coefficient**	**σ std. error**	**F-statistic**	**p-value**
TOC	1566.627	600.132	2.610471	0.022782
Mz_{SED}	-2.27257	1.259871	-1.80381	0.096404
DCI	4986.582	3396.119	1.468318	0.167737
$\%finer_{63}$	-65.276	53.671	-1.21623	0.247282

4.5. Relationships between microplastic composition and DCI

This section examines microplastic composition (polymer density and grain shape) in relation to depositional capacity (DCI) across facies.

A binned mean trend plot with error bars (95% CI) combined with level regression statistics show the relationship between mean polymer density and DCI per reclassified MP particle shape (Fig. 11). For all shapes besides rods depicting polymer density decreasing with increasing DCI for rod-shaped particles (β = -0.277, $R^2 = 0.16$, $p < 0.001$, ρ = -0.39), virtually

none ($R^2 \approx 0 – 3\%$) of the variance is explained by the regression despite detectable slope ($p < 0.05$ for all shapes except spheres). Thus, statistically DCI explain little to none of the variability in polymer density per shape but for rods. Nonetheless, visual inspection suggests that, in addition to rods, higher density thick blades and spheres occur in depositional facies exposed to strong hydraulic forcing (Fig. 11).

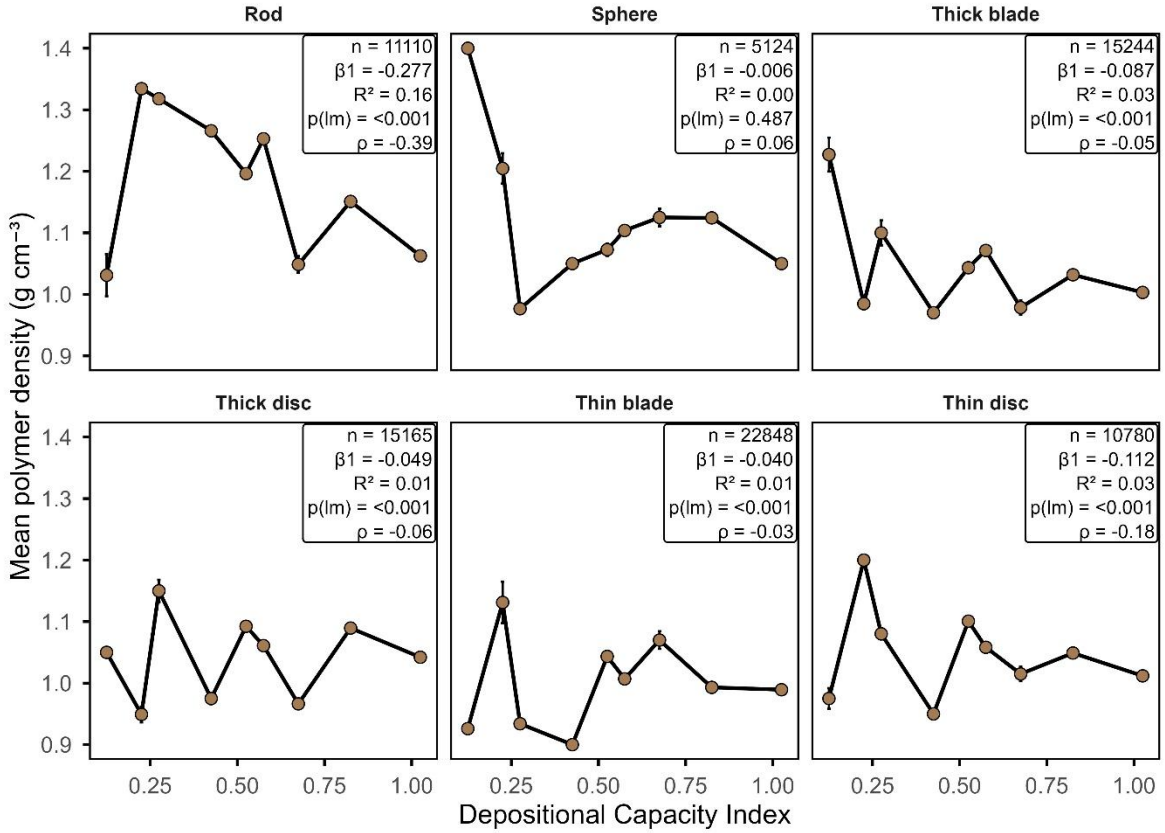

Fig. 11 Binned mean plots with 95% confidence interval showing mean polymer density (g cm^{-3}) derived from FTIR polymer identification plotted against DCI per reclassified microplastic grain shape. In the annotation box, p(lm) corresponds to the p-value when fitting a linear regression and ρ is the Spearman rho.

Shape proportions of total microplastics is plotted as clusters supported PERMANOVA compositional analysis using Bray-Curtis dissimilarity per facies annotated by their respective DCI value (Fig. 12). Rods are found in high proportions in sites with low DCI (high energy) i.e., main channel riverbed and plunge pool, while thin blades are found in higher proportions at facies characterised by low-energy regimes i.e., overbank, pocket pool, and vegetation-trapped deposits with backwater. Statistical results shows that the DCI

explains 9.6% of the variation in shape composition across all sites ($R^2 = 0.096$) and the relationship is not statistically significant (F = 1.59, p = 0.19). PERMANOVA results are not biased for tests of multivariate dispersion (betadisper) indicate no significant differences in dispersion among groups (F = 0.39, p = 0.69). There is also no significant correlation between Bray-Curtis dissimilarities of microplastic shape composition and differences in DCI as shown by a Mantel test (Spearman r = 0.065, p = 0.27, 9999 permutations).

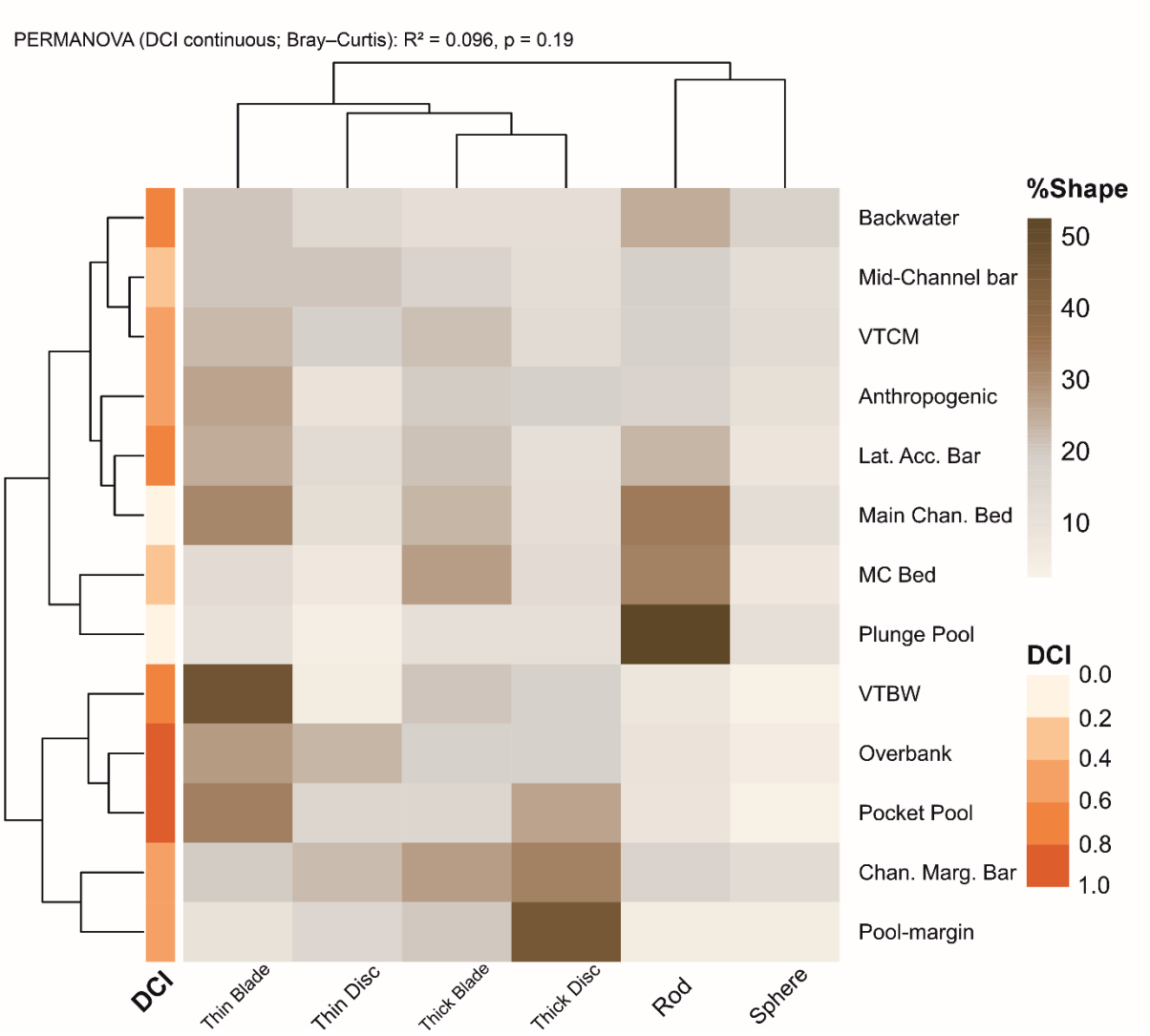

Fig. 12 Distance-based multivariate analysis showing proportions of microplastic shape composition variations along the depositional capacity index (DCI) gradient per facies.

The same four environmental predictors were tested simultaneously to explain variation in microplastic shape composition using PERMANOVA (Table 5). None of the predictors individually are significant, but Mz_{Sed} has the strongest effect (F = 1.74, p = 0.159). The

predictors collectively do not explain shape composition and the model is not statistically significant (F = 1.37, p = 0.183) despite 31% of the variance being explained (R^2 = 0.317).

Table 5: Term results from testing composition response against predictor variables using a distance-based redundancy analysis (dbRDA).

Variable	SS	F-statistic	p-value
TOC	0.079833	1.375576	0.262
Mz_{SED}	0.100959	1.739578	0.159
DCI	0.076258	1.313977	0.253
$\%finer_{63}$	0.060309	1.039153	0.391

5. Discussion

5.1. Facies-driven accumulation of microplastics

We have shown that characterizing facies with a semi-quantitative index of depositional capacity based on hydraulic exposure and sheltering provides a predictor for microplastic accumulation in river sediments (R^2 = 0.78, p = 1.3e-05). Facies with low DCI and high connectivity such as the mid-channel bar (1,952.6 MP kg^{-1}), plunge pool (1,064.3 MP kg^{-1}) or throughflow-exposed riverbed (353.6 MP kg^{-1}) largely contrast with high DCI and low connectivity facies such as the “metal bath” (6104.3 MP kg^{-1}), overbank deposits (8,794.3 MP kg^{-1}), pocket pool (14,664.3 MP kg^{-1}) or the backwater zone upstream of a debris dam at the river mouth (15,544.3 MP kg^{-1}). The DCI provides a useful proxy for sediment connectivity by integrating channel morphology and hydraulic conditions that control sediment transfer. However, this pattern holds only under the previously defined microplastic availability conditions, as upstream samples and those from the autumn 2025 campaign lack elevated microplastic concentrations. Positive significant correlations also exist between microplastic abundance and silt/clay content (R^2 = 0.33, p = 0.016) and TOC (R^2 = 0.59, p = 0.00032). Van Daele et al. (2024) found stronger correlations for both silt/clay content (R^2 = 0.65, $p < 0.01$) and TOC (R^2 = 0.78, $p < 0.001$) in riverbed sediments along a transect of the

meandering Lys River. A strong correlation with silt/clay content ($R^2 = 0.74$, $p = 0.001$), but no correlation with TOC was found in the Warnow estuarine sediments (Enders et al., 2019). On the contrary, microplastic abundance has been reported to correlate strongly with TOC but not with sediment grain size in the Thames and Medway estuaries ($R^2 = 0.71–0.96$; Trusler et al., 2024), with comparable patterns observed on the North-East Atlantic continental shelf (Maes et al., 2017). Removing outliers increases the correlation between microplastic abundance and silt/clay content to $R^2 = 0.69$, indicating that the relationship is driven by few observations. Multiple linear regression identifies TOC as the only significant predictor of microplastic abundance, suggesting that the DCI effectively captures organic matter deposition controlling local microplastic accumulation. Nevertheless, hydraulic exposure, sheltering and grain-size characteristics of fluvial facies likely also influence microplastic retention as they influence organic matter deposition. The most sheltered facies (pocket pools) show very high contamination (14,464.3 MP kg^{-1}), comparable to fine-skewed vegetation-trapped deposits near the river mouth (15,554.3 MP kg^{-1}), the latter likely influenced by inputs from the Mödlingbach upstream (Fig. 1). Both sites have high TOC values: 4.26 and 7.39% respectively.

The depositional capacity index can only partly explain the waning microplastic signal from April to October 2025. For example, it helps explain the sharp decrease at KT4.3S (channel-margin bar), where low bed roughness due to bed paving beneath the bridge reduces retention. However, the overall decline in microplastic concentrations more likely reflects the high hydraulic reactivity and flushing capacity of the channel, combined with dilution by newly deposited, relatively uncontaminated fine-grained sediments. High inter-annual variability in plastic mobilisation and decrease in microplastic abundance have been emphasized before (Hurley et al., 2018; Roebroek et al., 2021)

5.2. Relationship between microplastics and sediment grain sizes

The correlation between microplastics Mz and sediment Mz is perfectly linear and significant (R^2 = 0.99, p = 6.47e-16) with Mz_{MP} = 83.274 + 0.328 Mz_{SED} (Fig. 8). This relationship highlights that (1) microplastics are typically right-skewed, reflecting the progressive fragmentation of larger particles into smaller size classes (e.g. Enders et al., 2015), (2) microplastics are stored in bulk sediments that are about 3.3 times larger in their long-axis on average, (3) microplastics are responding to the same energy gradient and hydraulic sorting as natural sediments, (4) microplastics are subjected to facies-selective sorting. If microplastics were deposited primarily through density-sorting at the facies scale, a systematic sorting according to their polymer density and a weaker correlation with sediment grain-size statistics would be observed. Such systematic size correlation has not previously been described. A moderate positive relationship was observed between microplastic concentration and sediment sorting (Spearman's ρ = 0.46, p = 0.061), although the relationship was not statistically significant. The trend suggests that MP accumulation may be favoured in more poorly sorted depositional environments.

In the present study, the relatively small proportion of high-density microplastics (>1.15 g cm^{-3}; 19.4%) did not produce any clear relationship with sediment grain size. Previous studies report mixed relationships between microplastics and sediment grain size. Enders et al. (2019) found strong positive correlations between high-density microplastics and fine sand, although the plastics were much larger (>1 mm) than the associated sediment fraction. In coral reef sediments, Widiaratih et al. (2025) observed a negative correlation between plastic abundance and coarse sediments (>500 μm), suggesting that medium sand may act as an optimal trap for smaller particles. Similarly, Fenn et al. (2025) reported an inverse relationship between mean microplastic fragment size and sediment φ values (r_s = −0.668, p = 0.006), indicating larger plastics occur in coarser sediments. In contrast, Zhang et al. (2022) showed that microplastic abundance and polymer diversity in deep-marine sediments increase

with the mean grain size of detrital sediments, suggesting that transport processes may exert stronger control on deposition than interstitial pore-space trapping.

Accounting for these results, microplastic (MP) retention is primarily controlled by pore-space accommodation and transport processes, except for high-density MP, whose higher settling velocities promote accumulation in finer sediments, as observed by Enders et al. (2019).

5.3. Microplastic composition and deposition

Assuming polymer density is constant between manufacturing and sampling after deposition, polymer density is largely independent of depositional connectivity (Fig. 11). However, microplastic density can increase through biofouling involving organic matter growth on the surface, and through flocculation with suspended clay and surfactants reducing buoyancy and increasing settling (Kaiser et al., 2017; Sutherland et al., 2023). It is known that metals such as manganese and iron can sorb to biofilms covering microplastics increasing their mass (Leiser et al., 2020). The formation of biofouling is also density or polymer specific as it was shown that biofilms growth is more important on PET and PS particles than PE and PP (Leiser et al., 2025) and PS is particularly responsive over time exhibiting high biofilm mass growth and concordant high settling velocity after 60 days of incubation (Vercauteren et al., 2025). In a eutrophic river (similar conditions downstream a WWTP), it was shown that MP with density slightly less than water (PE and PP) rapidly sink due to biofouling and that smaller particles sink faster than larger ones for sizes down to 100 µm (Liu et al., 2022). The most common polymer in the present study are PS (35.4%), PE (16.4%), and PP (15.4%) which have density below water or slightly above for PS. The average particle is 218.3 µm, when excluding rods is 150.1 µm. The high proportion of PS of relatively small particle size

offer the right conditions for biofouling and increasing the density and settling velocity of microplastics in this study.

The depositional connectivity index (DCI) does not strongly influence microplastic shape composition (Fig. 12) and is also not significantly controlled by sediment texture, organic content, or the fine-grained sediment fraction (Table 5). Shapes are largely defined by their fragmentation processes, source material, and transport history, all of which are not directly constrained. In terms of deposition, applying the shape-based reclassification of microplastics as sediment (Russell et al., 2025), using either four or six categories as revised in this study, does not provide additional explanatory value.

5.4. Implications for microplastic transport in rivers

5.4.1. Analogy to natural sediments

Building on the discussion of microplastic abundance, composition, and sorting presented above, the following section provides a tentative interpretation.

For most particle shapes, once microplastics become negatively buoyant through biofouling, the influence of their initial polymer density may become secondary to local depositional hydraulics. This may explain the absence of a clear sorting relationship between depositional capacity (DCI) and polymer density for most shapes. Rods, however – the only morphology showing a detectable response to their initial density (Fig. 10) – are inherently highly anisometric and likely experience higher drag coefficients than more equant particles (e.g. Liu et al., 2022). As a result, rods may be less hydraulically homogenized by depositional processes than the other shapes. Their cylindrical geometry and high aspect ratio may lead to more shape-specific settling behaviour and a weaker overprinting by processes such as biofouling or aggregation, allowing the signal of their intrinsic polymer density to remain

more detectable. In addition, the elongated morphology of rods may promote selective sorting relative to bulk sediments through orientation and flow effects during transport.

The absence of a correlation between primary polymer density and depositional capacity, together with the high proportion of small PS particles and buoyant polymers such as PE and PP that are susceptible to density modification through biofouling and flocculation, and the observed sediment-like hydraulic sorting independent of particle shape, suggests that once microplastics settle within riverbed sediments they largely respond to the same hydraulic processes that control natural sediment deposition.

5.4.2. A highly anthropogenic polluted river

The Krotenbach River is highly polluted with values up to around 15,000 MP kg^{-1} observed in two low-energy facies ($Mean_{April} \pm SD = 4{,}719.9 \pm 4{,}644.5$ MP kg^{-1}). In comparison, channel margin sediments from six rivers in Shanghai showed abundance of 802±594 MP kg^{-1} (Peng et al., 2018), while similar facies from the River Rhine showed between 228–3,763 MP kg^{-1} (Klein et al., 2015). Crew et al. (2020) found 832±150 MP kg^{-1} in river sediments of the St Lawrence River, arguing to be among the highest recorded concentration globally. MP concentrations may be lower in larger rivers due to source integration and dilution, whereas smaller rivers like the Krotenbach are dominated by local inputs (e.g. Büngener et al., 2024).

The microplastics found in the Krotenbach are likely resulting from the fragmentation of larger plastic material as shown in Fig. 4. These plastics are the same type of primary industrial microplastics produced by Borealis as observed downstream the River Schwechat in water samples from the Danube (Austria) (Lechner et al., 2014). The WWTP is the likely point source of microplastic release in the Krotenbach. It has been previously shown that microplastics increase downstream WWTPs (Kay et al., 2018; Woodward et al., 2021). Over a decade later, microplastics in Austria still fall under the same legislation as highlighted by

Lechner and Ramler (2015) characterizing microplastics as part of the total suspended solids (TSS) that can be released through wastewater discharges, which effluent benchmark is a rate of 30 mg L^{-1}. Theoretically, with a daily volume discharge of 18,000 m^3, the Mödling WWTP could potentially pour up to 540 kg of TSS per day, all of which could legally be plastics. This corresponds to 197.1 t per year or 3.41 million 1 litter PET bottles per year (brand: Vöslauer®; mass (per bottle) = 57.7 g).

Microplastic concentration data for October stresses the importance of seasonality effect on microplastic storage in the river sediments. The Krotenbach is a highly anthropogenic single thread channelized stream, characterised by riverbeds depleted in fine sediment exhibiting low embeddedness. All the conditions exacerbate the high reactivity and efficiency of the channel to transport fine-grained material including microplastics. Such rivers as the Krotenbach are often overlooked and may represent major but underrecognized pollution vectors and should therefore be prioritized in remediation strategies.

6. Conclusion

Microplastics appear to undergo hydraulic size compensation relative to natural grains during transport, resulting in a systematic relationship between microplastic and sediment grain size. Their abundance is primarily controlled by depositional environments that favour the retention of organic matter, suggesting co-accumulation with organic-rich fine sediments. However, microplastic composition in terms of particle shape (except rods) and polymer density appears to not be controlled by environmental factors such as sediment grain size distribution, organic matter content, and sedimentary facies. These field observations indicate that sedimentary depositional environments, rather than intrinsic microplastic properties such as shape and density, exert the primary control on microplastic deposition in river sediments.

Overall, the Depositional Capacity Index (DCI) provides a simple, field-based approach for identifying microplastic hotspots in riverine environments.

CRediT authorship contribution statement

Samuel Roudbar: Conceptualization, Methodology, Investigation, Formal analysis, Writing – original draft, Writing – review and editing, Visualization, Project administration

Daniel Le Heron: Supervision, Conceptualization, Writing – review and editing

Michael Wagreich: Supervision, Conceptualization, Writing – review and editing, Resources, Funding acquisition

Ronald Pöppl: Supervision, Conceptualization, Writing – review and editing, Funding acquisition

Declaration of competing interest

The authors declare no conflicts of interest.

Acknowledgements

I would like to thank Dieter Mader (University of Vienna) for providing generously and flexibly all the liquid nitrogen required to run the FTIR microscope, Veronika Koukal (University of Vienna) for sharing her insights into building the microplastic extraction and analysis methods, Ahmed Ali (El Minia University, Egypt) for helping with the manual grain size analysis, Polly Crowther (University of Trieste) for kindly assisting the main fieldwork campaign, and Dean Velikov (University of Vienna) for the insightful and valuable advice when developing the microplastic extraction method. This project was funded by the University of Vienna (Emerging Field Grant of the Faculty of Earth Sciences, Geography and Astronomy), the Vienna Science and Technology Funds (WWTF ESR20-027) and the Austrian Academy of Sciences, ESS International Programs UNESCO IGCP 732.

Data availability statement

The data that supports the findings of this study are available in the supplementary material of this article.

References

Allen, S., Allen, D., Phoenix, V. R., Le Roux, G., Durántez Jiménez, P., Simonneau, A., ... and **Galop, D.** (2019). Atmospheric transport and deposition of microplastics in a remote mountain catchment. *Nature geoscience*, *12*(5), 339-344.

Anderson, M. J. (2001). A new method for non-parametric multivariate analysis of variance. *Austral ecology*, *26*(1), 32-46.

Andrady, A. L. (2011). Microplastics in the marine environment. *Marine pollution bulletin*, *62*(8), 1596-1605.

Austrian Hydrographic Service, ***eHYD***. (n.d.) *Hydrographic data Austria*. Available at: https://ehyd.gv.at (accessed: 14 April 2026).

Best, J. (2019). Anthropogenic stresses on the world's big rivers. *Nature Geoscience*, *12*(1), 7-21.

Bracken, L. J., Turnbull, L., Wainwright, J., and **Bogaart, P.** (2015). Sediment connectivity: a framework for understanding sediment transfer at multiple scales. *Earth surface processes and landforms*, *40*(2), 177-188.

Bridge, J. S. (2009). *Rivers and floodplains: forms, processes, and sedimentary record*. John Wiley and Sons.

Büngener, L., Schäffer, S. M., Schwarz, A., and **Schwalb, A.** (2024). Microplastics in a small river: Occurrence and influencing factors along the river Oker, Northern Germany. *Journal of Contaminant Hydrology*, *264*, 104366.

Crew, A., Gregory-Eaves, I., and **Ricciardi, A.** (2020). Distribution, abundance, and diversity of microplastics in the upper St. Lawrence River. *Environmental Pollution*, *260*, 113994.

Croiset, C., Dhivert, E., Phuong, N. N., Grosbois, C., Zalouk-Vergnoux, A., Baltzer, A., and **Gasperi, J.** (2024). Exploring possible controlling factors of spatial distribution of microplastics in sediments of a river segment (Loire River, France). *Science of The Total Environment*, *956*, 177328.

De Frond, H., O'Brien, A. M., and **Rochman, C. M.** (2023). Representative subsampling methods for the chemical identification of microplastic particles in environmental samples. *Chemosphere*, *310*, 136772.

de Souza Machado, A. A., Kloas, W., Zarfl, C., Hempel, S., and **Rillig, M. C.** (2018). Microplastics as an emerging threat to terrestrial ecosystems. *Global change biology*, *24*(4), 1405-1416.

Enders, K., Lenz, R., Stedmon, C. A., and **Nielsen, T. G.** (2015). Abundance, size and polymer composition of marine microplastics≥ 10 μm in the Atlantic Ocean and their modelled vertical distribution. *Marine pollution bulletin*, *100*(1), 70-81.

Enders, K., **Käppler, A**., **Biniasch, O.**, **Feldens, P.**, **Stollberg, N.**, **Lange, X.**, and **Labrenz, M.** (2019). Tracing microplastics in aquatic environments based on sediment analogies. *Scientific Reports*, *9*(1), 15207.

Fenn, O. J., Walklett, E. J., and **Turner, A.** (2025). Relationships between sediment size distribution and microplastic abundance and characteristics along the strandline of a sandy embayment (Whitsand, Southwest England). *Marine Pollution Bulletin*, *213*, 117686.

Folk, R. L., and **Ward, W. C.** (1957). Brazos River bar [Texas]; a study in the significance of grain size parameters. *Journal of sedimentary research*, *27*(1), 3-26.

Geologische Bundesanstalt Österreich (2021): Geodaten - Blatt 58 Baden (1:50.000). Tethys RDR, Geologische Bundesanstalt (GBA), Wien (https://doi.org/10.24341/tethys.29)

GeoSphere Austria (2025) Messstationen Jahresdaten v2. GeoSphere Austria, Vienna. https://doi.org/10.60669/923n-p390

Ghinassi, M., Michielotto, A., Uguagliati, F., and **Zattin, M.** (2023). Mechanisms of microplastics trapping in river sediments: Insights from the Arno river (Tuscany, Italy). *Science of The Total Environment*, *866*, 161273.

Hurley, R. R., Woodward, J. C., and Rothwell, J. J. (2017). Ingestion of microplastics by freshwater tubifex worms. *Environmental science and technology*, *51*(21), 12844-12851.

Hurley, R., **Woodward, J.**, and **Rothwell, J. J.** (2018). Microplastic contamination of river beds significantly reduced by catchment-wide flooding. *Nature Geoscience*, *11*(4), 251-257.

Ibna Hafiz, A. M., Ahmadisharaf, E., Salehi, M., Farner, J., White, J. C., Zeng, E. Y., and **Nazari, B.** (2025). A review of processes and models for the export of microplastics from terrestrial to aquatic systems. *Wiley Interdisciplinary Reviews: Water*, *12*(1), e70004.

Jarosz, K., **Natkański, P.**, and **Michalik, M.** (2022). Microplastic extraction from the sediment using potassium formate water solution (H2O/KCOOH). *Minerals*, *12*(2), 269.

Kaiser, D., **Kowalski, N.**, and **Waniek, J. J.** (2017). Effects of biofouling on the sinking behavior of microplastics. *Environmental research letters*, *12*(12), 124003.

Kay, P., Hiscoe, R., Moberley, I., Bajic, L., and **McKenna, N.** (2018). Wastewater treatment plants as a source of microplastics in river catchments. *Environmental Science and Pollution Research*, *25*(20), 20264-20267.

Kiss, T., Gönczy, S., Nagy, T., Mesaroš, M., and **Balla, A.** (2022). Deposition and mobilization of microplastics in a low-energy fluvial environment from a geomorphological perspective. *Applied Sciences*, *12*(9), 4367.

Klein, S., Worch, E., and **Knepper, T. P.** (2015). Occurrence and spatial distribution of microplastics in river shore sediments of the Rhine-Main area in Germany. *Environmental science and technology*, *49*(10), 6070-6076.

Lebreton, L. C., Van Der Zwet, J., Damsteeg, J. W., Slat, B., Andrady, A., and **Reisser, J.** (2017). River plastic emissions to the world's oceans. *Nature communications*, *8*(1), 15611.

Lechner, A., Keckeis, H., Lumesberger-Loisl, F., Zens, B., Krusch, R., Tritthart, M., ... and **Schludermann, E**. (2014). The Danube so colourful: a potpourri of plastic litter outnumbers fish larvae in Europe's second largest river. *Environmental pollution*, *188*, 177-181.

Lechner, A., and **RamLer, D.** (2015). The discharge of certain amounts of industrial microplastic from a production plant into the River Danube is permitted by the Austrian legislation. *Environmental Pollution*, *200*, 159-160.

Legendre, P., and **Anderson, M. J.** (1999). Distance-based redundancy analysis: testing multispecies responses in multifactorial ecological experiments. *Ecological monographs*, *69*(1), 1-24.

Leiser, R., **Wu, G. M., Neu, T. R.**, and **Wendt-Potthoff, K.** (2020). Biofouling, metal sorption and aggregation are related to sinking of microplastics in a stratified reservoir. *Water research*, *176*, 115748.

Li, W., Zu, B., Yang, Q., Huang, Y., and **Li, J.** (2022). Adsorption of lead and cadmium by microplastics and their desorption behavior as vectors in the gastrointestinal environment. *Journal of Environmental Chemical Engineering*, *10*(3), 107379.

Liro, M., Zielonka, A., Hajdukiewicz, H., Czajka, A., Mikuś, P., Dzida, J., and **Russell, C.** (2025). Rivers as microplastic factories. *Environmental Research Letters*, *20*(5), 051005.

Liu, S., **Huang, Y.**, **Luo, D.**, **Wang, X.**, **Wang, Z., Ji, X.**, ... and **Shang, X.** (2022). Integrated effects of polymer type, size and shape on the sinking dynamics of biofouled microplastics. *Water Research*, *220*, 118656.

Lofty, J., Valero, D., Wilson, C. A., Franca, M. J., and **Ouro, P.** (2023). Microplastic and natural sediment in bed load saltation: Material does not dictate the fate. *Water Research*, *243*, 120329.

Maes, T., Van der Meulen, M. D., Devriese, L. I., Leslie, H. A., Huvet, A., Frère, L., ... and **Vethaak, A. D.** (2017). Microplastics baseline surveys at the water surface and in sediments of the North-East Atlantic. *Frontiers in Marine Science*, *4*, 135.

Miall, A. (2014). *Fluvial depositional systems* (Vol. 14, p. 316). Cham: Springer International Publishing.

Monclús, L., Arp, H. P. H., Groh, K. J., Faltynkova, A., Løseth, M. E., Muncke, J., ... and Wagner**, M.** (2025). Mapping the chemical complexity of plastics. *Nature*, *643*(8071), 349-355.

Office of the Lower Austrian Provincial Government (Amt der Niederösterreichischen Landesregierung), GeoShop NÖ. Digital elevation model / orthophoto data. Available at: https://geoshop.noel.gv.at

Peng, G., Xu, P., Zhu, B., Bai, M., and **Li, D.** (2018). Microplastics in freshwater river sediments in Shanghai, China: a case study of risk assessment in mega-cities. *Environmental Pollution*, *234*, 448-456.

Poeppl, R. E., Keesstra, S. D., and **Maroulis, J.** (2017). A conceptual connectivity framework for understanding geomorphic change in human-impacted fluvial systems. *Geomorphology*, *277*, 237-250.

Poeppl, R. E., Perez, J. E., Fergg, H., and **Morche, D.** (2024). Introducing indices to assess the effects of in-stream large wood on water and sediment connectivity in small streams. *Geomorphology*, *444*, 108936.

Pohl, F., Eggenhuisen, J. T., Kane, I. A., and **Clare, M. A.** (2020). Transport and burial of microplastics in deep-marine sediments by turbidity currents. *Environmental science and technology*, *54*(7), 4180-4189.

Roebroek, C. T., **Harrigan, S.**, **Van Emmerik, T. H.**, **Baugh, C., Eilander, D.**, **Prudhomme, C.**, and **Pappenberger, F.** (2021). Plastic in global rivers: are floods making it worse?. *Environmental Research Letters*, *16*(2), 025003.

Rohais, S., Armitage, J. J., Romero-Sarmiento, M. F., Pierson, J. L., Teles, V., Bauer, D., ... and **Pelerin, M.** (2024). A source-to-sink perspective of an anthropogenic marker: a

first assessment of microplastics concentration, pathways, and accumulation across the environment. *Earth-Science Reviews*, *254*, 104822.

Russell, **C. E.**, **Pohl, F.**, and **Fernández, R.** (2025). Plastic as a sediment–a universal and objective practical solution to growing ambiguity in plastic litter classification schemes. *Earth-Science Reviews*, *261*, 104994.

Schneidewind, U., Nel, H. A., Drummond, J., Kukkola, A., Brekenfeld, N., Chetwynd, A. J., ... and **Krause, S.** (2025). Sediment-Water Interfaces as Traps and Sources of Microplastic Fragments and Microfibers─ Insights from Stream Flume Experiments. *ACS Esandt Water*, *5*(11), 6567-6578.

Schumm, S. A. (1985). Patterns of alluvial rivers. *Annual Review of Earth and Planetary Sciences, Vol. 13, p. 5*, *13*, 5.

Scientific Polymer Products Inc. (n.d.). *Density of polymers (by density).* https://scipoly.com/density-of-polymers-by-density/

Stadtgemeinde Mödling (2018). Umwelterklärung 2018 gemäß EMAS für den Standort Abwassereinigungsanlage Eumiwed. Mödling, Austria

Sutherland, B. R., Dhaliwal, M. S., Thai, D., Li, Y., Gingras, M., and **Konhauser, K.** (2023). Suspended clay and surfactants enhance buoyant microplastic settling. *Communications Earth and Environment*, *4*(1), 393.

Trusler, M. M., Moss-Hayes, V. L., Cook, S., Lomax, B. H., and **Vane, C. H.** (2024). Microplastics pollution in sediments of the Thames and Medway estuaries, UK: Organic matter associations and predominance of polyethylene. *Marine Pollution Bulletin*, *208*, 116971.

Van Daele, M., **Van Bastelaere, B.**, **De Clercq, J.**, **Meyer, I.**, **Vercauteren, M.**, and **Asselman, J.** (2024). Mud and organic content are strongly correlated with microplastic contamination in a meandering riverbed. *Communications Earth and Environment*, *5*(1), 453.

Vercauteren, M., **Lambert, S.**, **Hoogerwerf, E.**, **Janssen, C. R.**, and **Asselman, J.** (2024). Microplastic-specific biofilm growth determines the vertical transport of plastics in freshwater. *Science of the Total Environment*, *910*, 168399.

Waldschläger, K., and **Schüttrumpf, H.** (2019). Effects of particle properties on the settling and rise velocities of microplastics in freshwater under laboratory conditions. *Environmental science and technology*, *53*(4), 1958-1966.

Waldschläger, K., Lechthaler, S., Stauch, G., and **Schüttrumpf, H.** (2020). The way of microplastic through the environment–Application of the source-pathway-receptor model. *Science of the Total Environment*, *713*, 136584.

Waldschläger, K., Brückner, M. Z., Almroth, B. C., Hackney, C. R., Adyel, T. M., Alimi, O. S., ... and **Wu, N**. (2022). Learning from natural sediments to tackle microplastics challenges: A multidisciplinary perspective. *Earth-Science Reviews*, *228*, 104021.

Widiaratih, R., Sulhana, B. L. A., Putranto, A. B., Maslukah, L., Ismanto, A., Ayuningrum, D., ... and **Satya, E. D.** (2025). The correlation between microplastics characteristics and sediment grain size to microplastics accumulation in coral reef sediment in Gede Island, Rembang, Indonesia. *Journal of Ecological Engineering*, *26*(3), 200-212.

Woodward, J., Li, J., Rothwell, J., and **Hurley, R.** (2021). Acute riverine microplastic contamination due to avoidable releases of untreated wastewater. *Nature Sustainability*, *4*(9), 793-802.

Zhang, X., **Liu, Z., Zhao, Y., Ma, P., Colin, C.,** and **Lin, A. T.** S. (2022). Distribution and controlling factors of microplastics in surface sediments of typical deep-sea geomorphological units in the northern South China Sea. *Frontiers in Marine Science*, *9*, 1047078.

Zobkov, M., **Zobkova, M.**, **Galakhina, N.**, and **Efremova, T.** (2020). Method for microplastics extraction from Lake sediments. *MethodsX*, *7*, 101140.

Zuur, A. F., **Ieno, E. N.**, **Walker, N. J.**, **Saveliev, A. A.**, and **Smith, G. M.** (2009). *Mixed effects models and extensions in ecology with R* (Vol. 574, p. 574). New York: springer.